Proton transport in the short side chain perfluorosulfonic ionomer membranes

by

Xiaoyan Luo

B.Sc. (Science), Jinan University, 2007

THESIS SUBMITTED IN PARTIAL FULFILLMENT
OF THE REQUIREMENTS FOR THE DEGREE OF
MASTER OF SCIENCE

In the
Department of Chemistry
Faculty of Science

SIMON FRASER UNIVERSITY

Fall 2011

Approval

Name: **Xiaoyan Luo**

Degree: **Master of Science**

Title of Thesis: ***Proton transport in short side chain perfluorosulfonic ionomer membranes***

Examining Committee:

Chair: **Dr. Michael Eikerling**
Associate professor

Dr. Steven Holdcroft
Senior Supervisor
Professor

Dr. Zuo-Guang Ye
Supervisor
Professor

Dr. Robert A. Britton
Associate Professor
Supervisor

Dr. Daniel B. Leznoff
Internal Examiner
Professor
Department of Chemistry

Date Defended/Approved: December 5, 2011

Declaration of
Partial Copyright Licence

Abstract

The influence of ion exchange capacity (IEC) on the water sorption properties of high IEC, short side chain (SSC) perfluorosulfonic acid (PFSA) ionomer membranes, and the relationships between water content, proton conductivity, proton mobility, water permeation, and oxygen diffusion were investigated. Transport properties of SSC ionomer membranes were compared with a series of long side chain (LSC) PFSA membranes. At 25 °C, fully-hydrated SSC ionomer membranes were characterized as possessing higher water contents, moderate λ values, high analytical acid concentrations, and moderate conductivity than LSC PFSA membranes; but lower than anticipated effective proton mobility. Complementary measurements of water permeability and oxygen diffusion also revealed lower than expected values given their much higher water contents than LSC analogues. Potential benefits afforded by reducing the side chain length of PFSA ionomer membranes, such as increased crystallinity, higher IEC, and high hydrated acid concentration were diminished by a less-developed, disorganized hydrophilic percolation network, which provides a motivation for future improvements of transport properties for this class of material.

Keywords: IEC, proton transport, PFSA, SSC, hydrophilic network

Dedication

To everyone who has helped me throughout my studies

To my family

Acknowledgements

I would like to thank:

My senior supervisor, Prof. Steven Holdcroft, for allowing me to work under his supervision and for his guidance throughout my studies.

My supervisory committee Prof. Robert A. Britton and Prof. Zuo-Guang Ye for their helpful ideas to improve my research.

My internal examiner Prof. Daniel B. Leznoff for taking the time to read my thesis.

Prof. Yongming Zhang for synthesising polymer materials used for this study.

Drs. Mahesh Kulkarni and Tim Peckham for useful discussions and suggestions.

Dr. Ana Mani for collecting the oxygen diffusion data for SSC-1.3 and Nafion® 211 membranes.

Drs. Ken Shi, Zhong Xie and Mr. Dave Edwards for support and technical guidance during the joint SFU-NRC collaborative research project.

Mr. Thomas Weissbach for helping with drawing graphical illustrations.

Past and present members of the Holdcroft research group for their friendship and making my Canadian student life interesting.

The British Columbia Innovation Council and the Natural Sciences and Engineering Research Council of Canada for financial support.

Table of Contents

List of Tables

List of Figures

Glossary

a_i	activity of the ion
AFC	alkaline fuel cell
AC	alternating current
CE	counter electrode
CV	cyclic voltammogram
DHE	dynamic hydrogen electrode
DMF	*N*,*N*-Dimethylmethanamide
DMFCs	direct methanol fuel cells
D_{O2}	oxygen diffusion coefficient/ cm^2s^{-1}
EIS	electrochemical impedance spectroscopy
FRA	frequency response analyzer
EW	equivalent weight
F	faraday's constant/ C mol^{-1}
f_i	degree of ion dissociation
IEC	ion exchange capacity
J_{LLP}	liquid-liquid permeation flux/ mol m^{-2} s^{-1}
LLP	liquid-liquid permeation
LVP	liquid-vapour permeation
LSC	long side chain
MCFC	molten carbonate fuel cell
N117	Nafion® 117
NR211	Nafion® 211
PAFC	phosphoric acid fuel cell
PEM	proton exchange membrane
PEMFC	proton exchange membrane fuel cell
PFSA	perfluorosulfonic acid
PFSI	perfluorosulfonated ionomer
PTFE	polytetrafluoroethylene
R_m	membrane resistance
RT	room temperature
SOFC	solid oxide fuel cell
SSC	short side chain
SANS	small angle neutron scattering
SAXS	small angle X-ray scattering
T	membrane thickness/ mm

TEM	transmission electron microscopy
TFE	tetrafluoroethylene
Tg	glass transition temperature/ °C
XRD	x-ray diffraction
X_v	water volume fraction
VVP	vapour-vapour permeation
V_{water}	volume of water in the membrane/ cm^{-3}
V_{dry}	dry volume of membrane/ cm^{-3}
W	width of membrane/ mm
W_{wet}	wet sample mass/ g
W_{dry}	dry sample mass/ g
WE	working electrode
ρ	density of membrane / g cm^{-3}
λ	water content of the membrane-number of water molecules per sulfonic site(H_2O/ SO_3H)
σ_e	electrical conductivity/ Scm^{-1}
σ_i	ionic conductivity/ Scm^{-1}
σ_{H+}	proton conductivity/ Scm^{-1}
η	density of charge carriers
μ	mobility/ $cm^2\ V^{-1}s^{-1}$
μ_e	electrical mobility/ $cm^2\ V^{-1}s^{-1}$
μ'_{H+}	effective proton mobility/ $cm^2\ V^{-1}s^{-1}$
Z_i	number of charges

1. Introduction

1.1. Fuel cell

A fuel cell is a device which directly converts chemical energy into electrical energy with high efficiency. Due to the tremendous increase in worldwide demand for energy as well as the environmental impact of greenhouse gases, fuel cells are seen as efficient low emission alternatives to hydrocarbon combustion engines for the transport industry.[1-3] Moreover, a fuel cell generates energy continuously as long as the reactants are being supplied, whereas in the case of batteries, the total amount of electrical energy produced is determined by the amount of reactant stored in the device. Fuel cells have been used in many applications, for mobile, stationary and portable power.[4-5] However, high cost and low durability are the issues that hinder fuel cell commercialization.[6]

The fuel cell concept was first demonstrated by William R. Grove, a British physicist in 1839.[7] Due to technological difficulties, fuel cell development received significant attention on the 1954 space mission by NASA, where there was a need to use fuel cells as compact electrical generators.[8] The polymer electrolyte fuel cell was first used in the later missions of the Gemini program. Table 1.1 summarizes the five major types of fuel cells according to their electrolyte, conducted ion, operating temperature and application.

Table 1.1 Comparison of common fuel cell technologies[6, 9-10]

Fuel cell type	Common electrolyte	Conducted ion	Operating temperature range(°C)	Application
Solid Oxide (SOFC)	Ceramic membrane	O^{2-}	500-1000	-Auxiliary power -Electric utility -Large distributed power generation
Molten Carbonate (MCFC)	Carbonate of Na^+, K^+, Li^+	CO_3^{2-}	620-660	-Constant power
Phosphoric Acid (PAFC)	Concentrated phosphoric acid	H^+	150-220	-Distributed generation
Alkaline (AFC)	Base solution	OH^-	90-100	-Military -Space
Proton Exchange Membrane (PEMFC)	Proton exchange membrane	H^+	20-100	-Back-up power -Portable power -Small distributed generation -Transportation

1.2. Proton exchange membrane fuel cell

Compared to other type of fuel cells, the proton exchange membrane fuel cell (PEMFC) operates at a relatively low temperature (typically 60-80 °C) and allows for a quick start-up.[11] In addition, PEMFC generates more power for a given volume or weight than any other type of fuel cell.[7] Their high-power density characteristic makes them compact and light weight. Another advantage is that the electrolyte, being a solid material, simplifies the sealing of the anode and cathode gases, thus, making PEMFC less expensive to manufacture.[7] The main challenge for the wide scale commercialization of PEMFC is a reduction in system cost. Expensive polymer membranes and noble-metal catalysts contribute to their high cost.[12]

Hydrogen/oxygen (H_2/O_2) PEMFC and direct methanol fuel cells (DMFCs) are two main types of PEMFC that use polymeric proton exchange membranes as an electrolyte. Compared to (H_2/O_2) PEMFC, DMFCs have slower oxidation kinetics and significant fuel permeation.[13] The main components of a single (H_2/O_2) PEMFC are illustrated in Figure 1.1. It consists of an anode, a cathode and an electrolyte. During operation, humidified hydrogen is fed to the anode and is electro-catalytically oxidized. Electrons and protons are liberated in the oxidation reaction. Electrons flow through an outer circuit to power the load. Protons are transported through the polymer membrane and react with oxidant (i.e., O_2) at the cathode. Water is the by-product. In PEMFC, the polymer electrolyte acts both as a proton transport medium and gas separator.

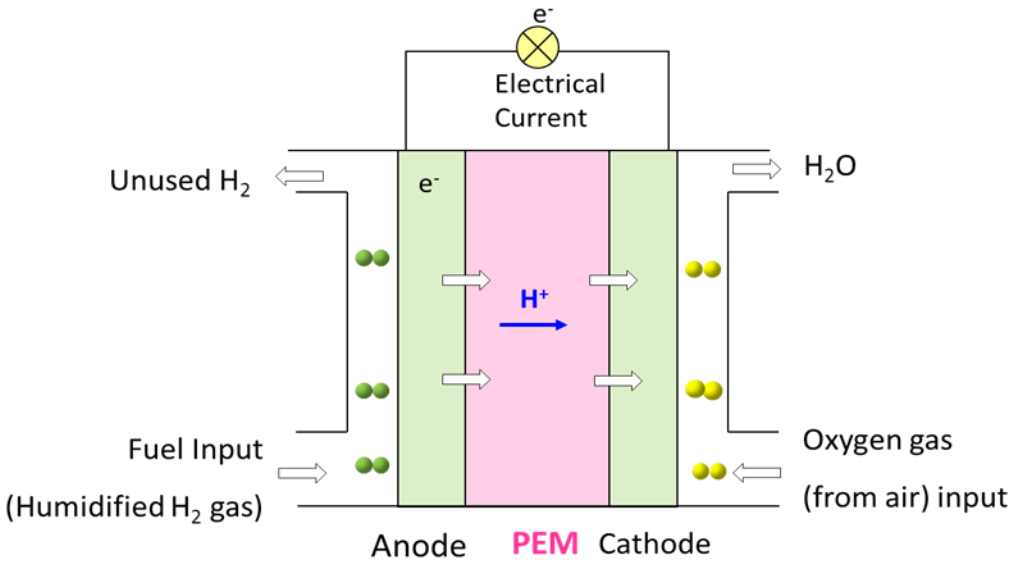

Figure 1.1 Schematic of an operating of proton exchange membrane fuel cell

1.3. Proton exchange membranes

A proton exchange membrane (PEM) is typically a thin film (<50 μm) made from an inert polymer that bears acidic groups.[11] This film selectively transports ions (H^+) from one electrode to the other. In addition, the PEM also serves as the electrode separator which completely blocks access to other ions and gaseous (i.e., hydrogen or oxygen). The requirements of a PEM are listed as follows: [12, 14-16]

- high proton conductivity
- high mechanical and chemical stability
- balanced water transport
- low fuel and oxidant cross-over
- electrical insulation

1.3.1. Nafion® membrane

While the first PEMFC used a membrane comprised of either a sulfonated phenolic resin or a sulfonated, cross-linked polystyrene electrolyte,[17] most commercial systems today use perfluorosulfonic acid (PFSA) ionomer. The higher stability of the C-F bond[18] compared to carbon-hydrogen bonds confers a high resistance to strongly acidic or oxidizing environments.[19] For several decades, Nafion®, commercialized by the E.I. Dupont Co. has been the benchmark PFSA ionomer membrane for low–to-medium temperature (25-80°C) PEMFC. PFSA is synthesized by copolymerization of a perfluorinated vinyl ether monomer with tetrafluoroethylene (TFE), resulting in the chemical structure given in Figure 1.2.[20] The equivalent weight (EW g mol^{-1}) and thickness of the material are often used to describe commercially available membranes. The EW is defined as the weight of dry Nafion® per mole of sulfonic acid groups when the material is in the H^+ form. For example Nafion® N117 represents a membrane prepared by melt extrusion of the sulfonyl fluoride form of the PFSA ionomer having 1100 EW and a thickness of 0.007 in. (175 µm). As a result of the extrusion process, membranes prepared using this technique have anisotropic swelling and conductivity which is lower in the extrusion direction.[21] Due to the difficulty of extruding membranes < 50 microns thick,[11] manufactures have recently turned to so-called “dispersion-cast” processes, wherefrom PFSA membranes are cast in their acid form from a dispersion of the ionomer in a mixture of alcohol and water. Nafion® NR211 used in this thesis work, was fabricated by dispersion casting with 1100 EW and was 0.001 in. (25 µm) thick.

Over the past decades, significant attention has been paid to reducing the thickness of membranes in order to reduce ionic resistance and increase the permeability of water.[22-23]

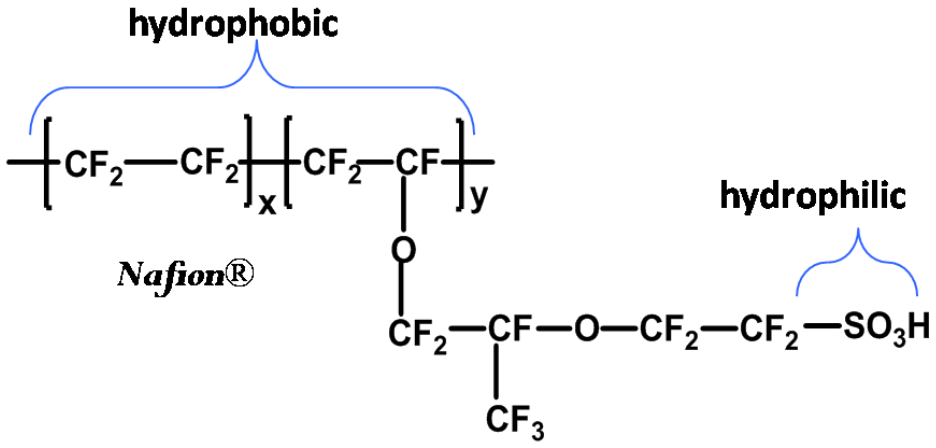

Figure 1.2 Chemical structure of Nafion®, typically x= 6–10 and y =1

Nafion® consists of a hydrophobic perfluorinated backbone, with pendent vinyl ether side chains terminated by a hydrophilic sulfonic acid group. The EW (g mol^{-1}) and therefore the proton conductivity are governed by the ratio of the two monomers. A higher sulfonated acid content results in a more hydrophilic membrane that can absorb more water, thereby providing higher proton conductivity, and hence greater power output from a fuel cell. However, raising the acid content too high compromises the membrane's mechanical properties because it swells excessively with water. For fuel cell applications, Nafion® membranes typically have equivalent weights of ~ 1000 to 1100 g mol^{-1}. While these membranes possess many desirable properties, they still suffer from poor proton conductivity under low relative humidities and high temperatures (> 90

°C).[24] A lower EW membrane is required for increased proton conductivity under hotter, drier conditions.

1.3.2. Short side chain membrane

In the 1980s, a promising class of PFSA ionomer was introduced by the Dow Chemical Co. This polymer was similar in structure to Nafion® but possessed a shorter pendent side chain, wherefrom this ionomer became known as short-side-chain (SSC) PFSA ionomer (See Figure 1.3), and correspondingly, Nafion® membrane referred to as a long side chain (LSC) PFSA ionomer.SSC ionomers can theoretically be prepared with lower EW, and hence higher fuel cell conductivity. Because for a given EW, more tetrafluoroethylene (TFE) units are present in the SSC *backbone*, compared to LSC analogues, providing a higher degree of crystallinity, and thereby improving the resistance of the membrane to swelling in water. Dow membrane, however, was commercially abandoned because of its complicated synthesis and high cost, despite improvements observed in fuel cell performance over LSC PFSA ionomer membranes.[25] Recently, Solvay Solexis developed an easier, cheaper synthetic route to the short side chain (SSC) PFSA ionomer. Membranes under the trade name, *Aquivion*® (-previously Hyflon® Ion), possess similar properties to the original Dow ionomer membranes,[26] and, compared to LSC PFSA analogues exhibit a higher degree of crystallinity, potentially enhanced proton conductivity and higher glass transition temperature (Tg)[27]– all of which collectively confer improved mechanical durability, greater fuel cell power output, and enable higher temperature operation. Figure 1.3 illustrates the chemical structure of different PFSA polymers reported in the literature and available commercially, showing

Aquivion® as the one possessing the shortest side chain among all.[28] 3M® was introduced by 3M Co. and Aciplex™ was developed by Asahi Kasei.

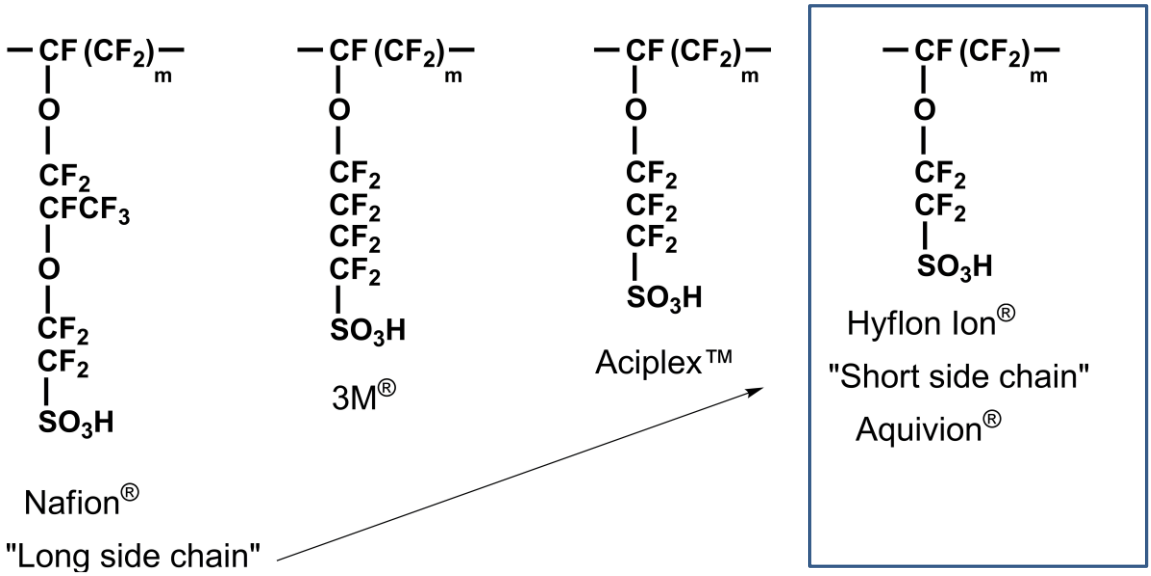

Figure 1.3 Structure of different PFSA ionomers commercially available, adapted from ref.[29]

(With the permission from WILEY-VCH Verlag GmbH&Co. KGaA, Copyright 2010).

1.4. Membrane morphology

Polymer morphology deals with the structure of polymer systems in the solid state and is studied because it strongly influences transport and mechanical properties. Membrane morphology largely depends on the polymer chemical structure and membrane fabrication conditions and is usually examined by small angle X-ray scattering (SAXS) and small angle neutron scattering (SANS).[30]

Long side chain (LSC) ionomer membranes such as Nafion® have been studied extensively over the last 25 years. The sulfonic acid functional group are known to aggregate to form hydrophilic domains that become hydrated in the presence of water. The tetrafluoroethylene (TFE) containing backbone forms crystallites, which contributes to the mechanical strength of the membrane and prevent the polymer from dissolving in water. Gierke et al. proposed a cluster-network model for the morphology of the water-saturated membrane as illustrated in Figure 1.4.[31] In this model, the ionic clusters swell and are connected by nanometer-scale channels, which provide a continuous path for proton transport. Although the cluster-network model initially gained wide acceptance, there appears no direct experimental evidence for the channels connecting the cluster in this model.

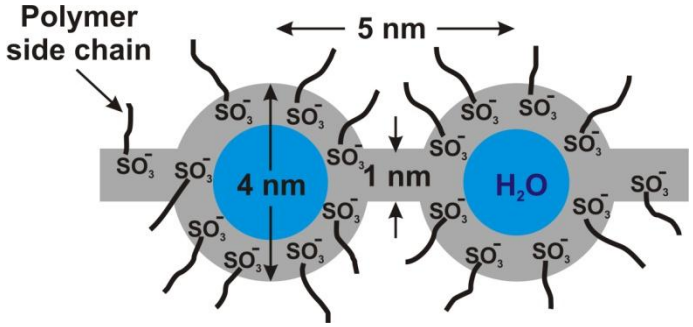

Figure 1.4 Schematic representation of ionic aggregates in PFSA ionomer membranes.(courtesy of Ref.[31])

Several other morphological models have since been reported.[32-33] More recently, Schmidt-Rohr and Chen developed a 3-D model that better matches published SAXS data for hydrated Nafion® membranes.[34] Based on their results, hydrated Nafion®

consists of bunches of parallel, cylindrical nano-sized water channels as illustrated in Figure 1.5. Strong molecular interactions between crystalline domains (polymeric backbones) are said to make the cylindrical walls stiff and stable.[2] Moreover, the cylinder diameter is much larger than that in other models, which explains the excellent transport properties of hydrated Nafion® to molecular species.[5]

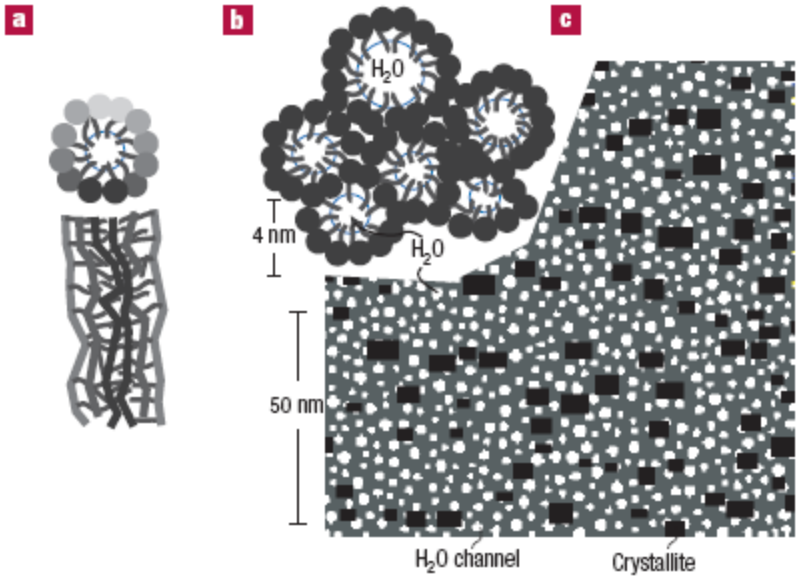

Figure 1.5 Illustration of parallel water-channel model for Nafion®, proposed by Schmidt-Rohr et al. (a) Schematic diagram of an inverted-micelle cylinder, with the polymer backbone on the outside and the ionic groups lining the water channel. (b) The cylinders are packed in hexagonal order. (c) Cross-section image of the Nafion® matrix. The cylindrical water channels are shown in white, the Nafion crystallites are shown in black and the non-crystalline Nafion matrix are shown as dark grey.

(Reprinted from ref[34] Copyright (2008) with permission from Elsevier.)

In spite of the numerous Nafion® models that have been proposed, the exact morphology of the water containing region, is still under debate[20] because of the

inhomogeneous nature of the membranes when hydrated. Nevertheless, these membrane models confirm that a continuous aqueous phase composed of "water channels" is formed due to phase incompatibility of hydrophobic back bone and hydrophilic side chain at a given level of hydration. Protons and water transport through these water channels. The shape of the water channels varies with the amount of water uptake by the membrane and the size of the channels are on the order of few nano-meters. The properties of the channels are determined by the equilibrium reached between the internal osmotic pressure of the clusters and the counteracting elasticity of the organic matrix.[35]

The morphology of short side chain (SSC) PFSA membranes is relatively unexplored. Moore et al. studied the Dow SSC PFSA membranes using SAXS, which revealed the presence of ionic clusters.[36] The size of these clusters was found to vary with EW and water content of the membranes. Gebel and Moore studied the same Dow SSC PFSA membranes using SAXS and SANS under dry and water swollen conditions. The presence of phase separated hydrophilic and hydrophobic domains was confirmed in both dry and wet states. Their study showed that SSC PFSA ionomer membranes have a similar morphology to that of Nafion®. Kreuer et al. investigated Dow SSC membranes and observed that there is a smaller degree of hydrophobic/hydrophilic separation as function of water content for SSC PFSA membranes in comparison to Nafion®. [37]

1.5. The state of the water in PEMs

In hydrated proton exchange membranes, water and protons are confined to nano-scale domains. Because the water is confined, its structure and properties are different from bulk water.[38] As illustrated in Figure 1.6 (a), in the center of the pore, water acts like bulk water. However, the water molecules outside of the pore center are strongly bound to the ionic groups (i.e., H^+) associated with the polymer. Reducing the humidity in the membrane reduces the amount of bulk water present in the pore and alters the size of the pore. As illustrated by the cartoon in Figure 1.6 (d), bulk water in the pore is lost and the remaining water is highly polarized and confined to very small regions.

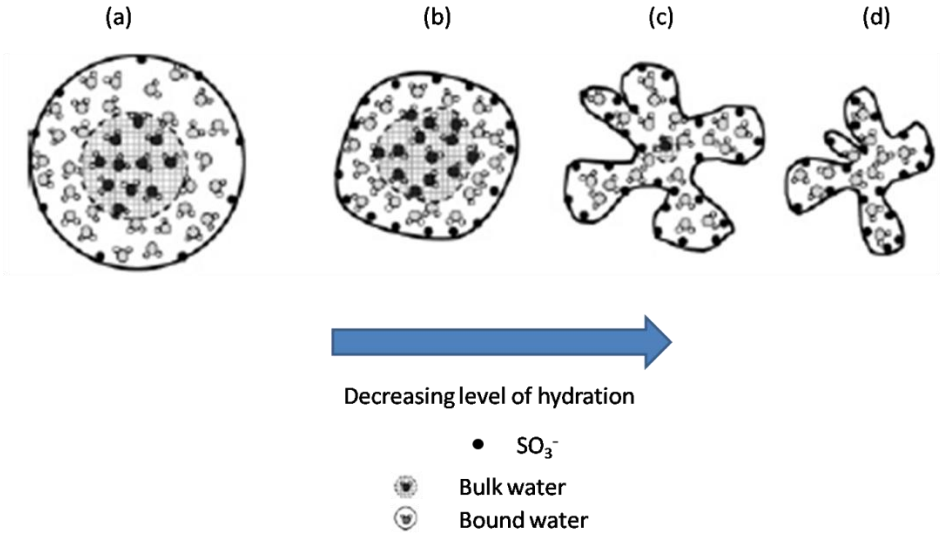

Figure 1.6 Schematic diagram illustrating the different types of water in the hydrophilic pore of a membrane.

(Adapted from ref.[38] with the permission of American Chemical Society, copyright 2006.)

1.6. Proton conductivity

Proton conductivity is a key parameter of a PEM as it directly influences the power output of the proton exchange membrane fuel cell (PEMFC). *Ex-situ* proton conductivity measurements provide a simple and quick evaluation of the ability of a membrane to transport protons. In addition, there exists a large body of literature on proton conductivity derived from ex-situ measurements, thus making comparisons between the proton conducting ability of different membrane systems possible. Furthermore, understanding the correlation between protons and water, and how they affect proton conductivity in the PEMs is an important factor in designing new membranes.

The proton conduction mechanisms in hydrated PEMs may be understood from a consideration of dissociation of the proton from the acidic site and, subsequent transport in the aqueous environment. When sulfonic acid groups became hydrated, they donate their protons to the water contained in the aqueous phase of the PEM. The degree of proton dissociation depends mainly on the water content of the membrane. For PFSI membranes, this can be estimated from studies of small molecules, such as triflic acid (CF_3SO_3H) for which the pKa is ~ -14.[39] Paddison and coworkers calculated that the dissociation of the proton in triflic acid occurs when the ratio of water molecules to sulfonic acid groups (H_2O/SO_3H), λ, is equal to 3 and that complete dissociation does not occur until λ= 6.[40] However, calculations by Eikerling et al. indicate that the minimum number of water molecules required for complete proton dissociation in Nafion® can be as low as 1, depending on the proximity of the tethered sulfonic acid groups.[41] The differences in the strength of the conjugate base (sulfonate anion) will also affect the

hydrogen bonding of the water molecules and the consequent transport of protons. This is particularly important for proton transport under conditions of minimal water content.

In the presence of water, protons are strongly associated with water molecules to form dynamic aggregates, such as, H_3O^+ (Hydronium ion); $H_5O_2^+$ (Zundel ion); and $H_9O_4^+$ (Eigen ion).[42-43] Under an applied electric field, protons are thought to migrate using three competing mechanisms: the "surface" mechanism; the "Grotthuss" mechanism; and the "vehicle" mechanism, schematically illustrated in Figure 1.7.[44] The transport mechanism in a membrane depends on the water content of the membrane. For the surface mechanism, protons "hop" between the sulfonic acid groups along the pore surface. The Grotthuss mechanism describes structured diffusion in the "water pool" where protons are transferred down a chain of hydrogen bonds followed by reorientation of the water dipoles (i.e.$H_5O_2^+$ and $H_9O_4^+$).The vehicle mechanism describes a classic molecular diffusion process. Water molecules are used as a vehicle to transport the protons while empty "vehicles" move in the opposite direction as schematically shown in Figure 1.8 (bottom).

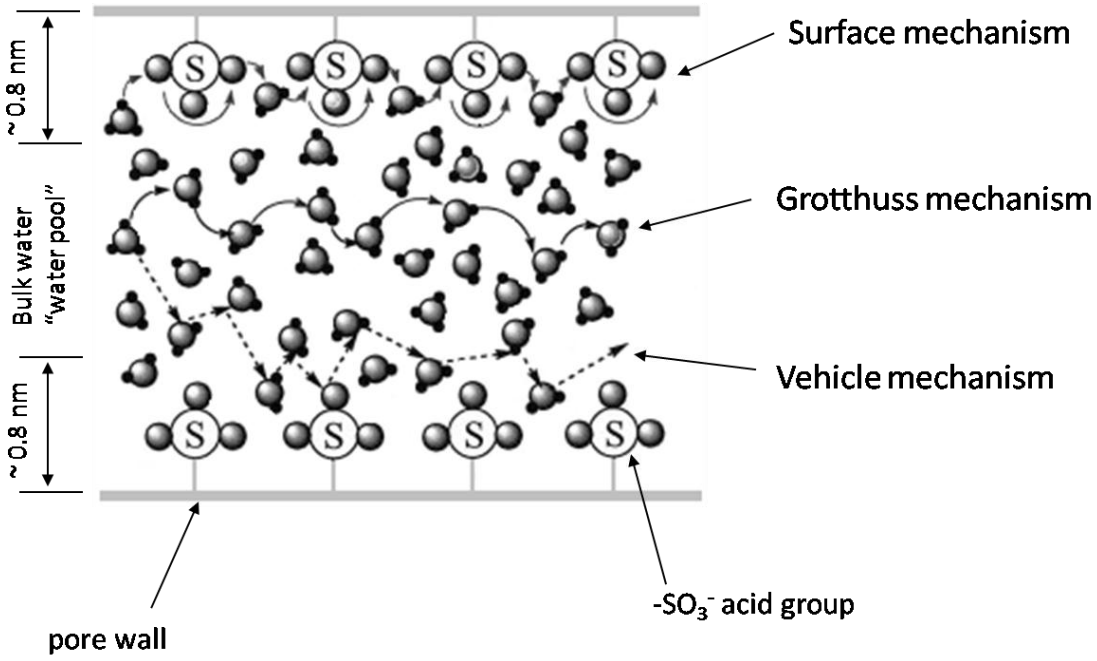

Figure 1.7 Simplified schematic of the structure and proton transfer in Nafion® in a fully hydrated state.

(Reproduced from ref [44] with the permission of John Wiley and Sons Inc., copyright 2006.)

Figure 1.8 Models of proton conduction. Top: Grotthuss Mechanism: protons are passed along the hydrogen bonds. Bottom: Vehicle Mechanism: protons are transported by H_2O.

(courtesy of Ref.[45])

A more thorough description of the Grotthuss mechanism was reported by Kreuer et al. as shown in Figure 1.9.[43] The breaking and reforming of hydrogen bonds provides a path for proton transport that is rapid due to the short, strong nature of hydrogen bonds. The rapid transformation between the Zundel ion and the Eigen ion is the reason for rapid proton transport in PEM, and thus proton conduction via the Grotthuss mechanism is faster than the vehicular transport of protons. As the Grotthuss mechanism relies on the rate of breaking and reforming of hydrogen bonds, any factors that affect the breaking and forming of hydrogen bonds will also affect proton transport. For example, as the rate of breaking and reforming of hydrogen bonds increases with temperature, transport by the Grotthus mechanism is also believed to increase. However, bulk water content in the membrane decreases with increasing temperature, and thus potentially there is a detrimental effect upon the rate of Grotthus mechanism.

Vehicle-type mechanisms are thought to increasingly predominate over Grotthuss-type mechanisms with increasing temperature.[42]

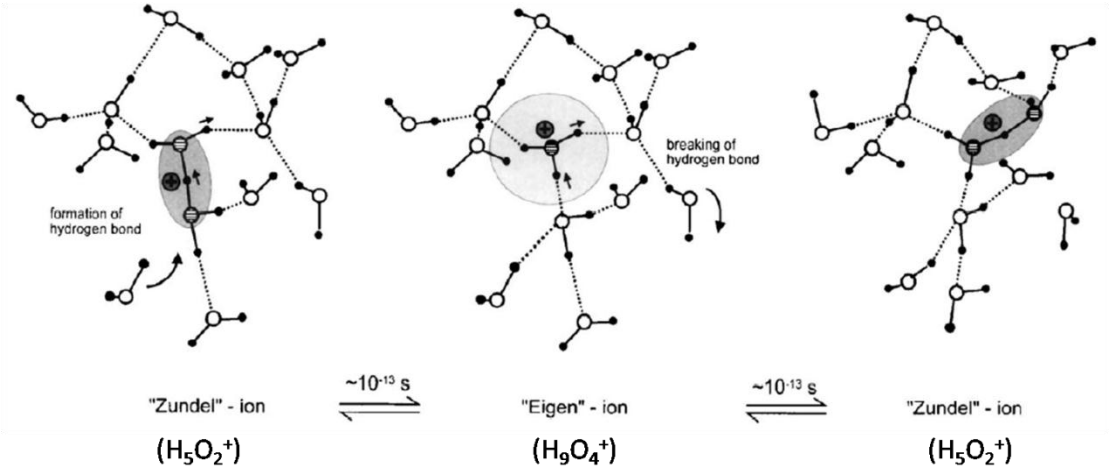

Figure 1.9 Schematic of Grotthuss mechanism in water. The shaded parts indicate proton transfer.

(Reprinted from ref.[43] with the permission of Elsevier, copyright 2000.)

1.6.1. Effective proton mobility

The mobility (μ, $cm^2\ V^{-1}s^{-1}$) of a charged particle is used to indicate how fast species move as a function of electric field strength. The general electrical conductivity, σ_e, is a function of the quantity of charge carriers in a given volume, η, and the mobility of those charge carriers, μ_e and their charge, e, (equation1-1).[46]

$$\sigma_e = \eta e \mu_e \qquad \textit{Equation 1-1}$$

This general relationship can be extended to conductivity of ionic systems (equation1-2). σ_i is the specific conductivity of the ion, F is Faraday's constant (96 485 C mol^{-1}), a_i is the activity of the ion, Z_i is the charge on the ion, and μ is the mobility.

$$\sigma_i = F a_i |Z_i| \mu_I$$ ***Equation 1-2***

The activity, a_i, can be defined using equation 1-3 where f_i is the degree of ion dissociation and C_i is the analytical concentration of the ion.

$$a_i = f_i C_i$$ ***Equation 1-3***

Equation 1-2 can be rewritten by the substitute a_i with f_i and C_i:

$$\sigma_i = F f_i C_i |Z_i| \mu_i$$ ***Equation 1-4***

Since f_i depends on both the pKa of the acid group and the water content of the proton exchange membrane (PEM), it is a difficult quantity to ascertain, especially in the case of PEMs which is highly heterogeneous. Hence the activity a_i is simplified as the analytical concentration of the ion ([-SO_3H]) in this work. In the case of proton mobility and the ion mobility becomes the "effective" ion mobility μ'. Z_i is equal to one and equation1-4 is expressed as the following equation 1-5.

$$\sigma_{H+} = F[-SO_3H]\mu'_{H+}$$ ***Equation 1-5***

The effective proton mobility can thus be estimated from the measurement of proton conductivity and [-SO_3H].[47]

There are many factors that affect effective proton mobility. One factor is the degree of acid dissociation. Water content, temperature and pKa of acid all affect this dissociation process. In an extreme case, if all the acid groups in the membrane remain undissociated, the effective mobility value is zero. Another factor is the degree of tortuosity of the water-saturated channels. Figure 1.10 is a schematic representation of the tortuorsity in PEMs. In comparison with A, the conduction pathway in B is more tortuous and contains dead ends.

Figure 1.10 Schematically diagram of proton conduction pathway in PEM (white = aqueous domains) where the degree of tortuosity of proton conduction pathway is greater in B than in A

The spatial proximity of neighboring acid groups in PEM may also play an important role in affecting proton mobility and may be a factor in surface mechanism where protons "hop" between the sulfonic acid groups along the pore surface. This is shown schematically in Figure 1.11 where the distance between acid groups in B is further than in A; thus, proton diffusion to transport in B may be less energetic.[19, 48] Closer proximity of the sulfonic acid groups along a pore wall may also be achieved by conformational changes in the backbone.[49]

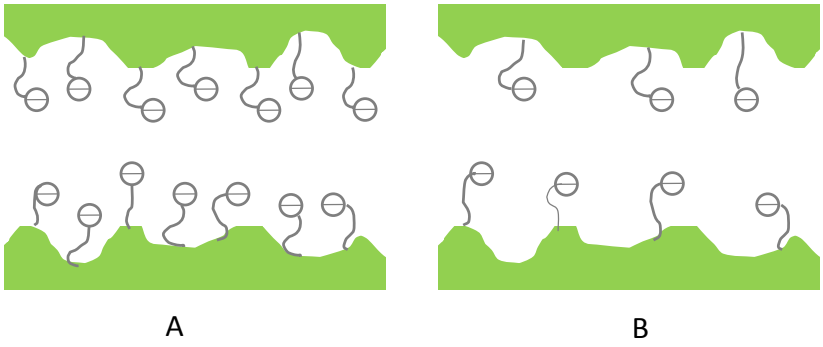

Figure 1.11 Spatial proximity of neighboring acid groups in a water saturated channel

Another factor that influences proton mobility is the size of proton channel. High proton mobility will be anticipated for larger proton channels. The stronger confinement of the water in the narrow channels leads to a significantly lower dielectric constant of the water of hydration(i.e., the water molecules are more tightly bound to each other and to the fixed sulfonate group).[35]

1.7. Thesis outline

For the past 40 years, long side chain (LSC) perfluorosulfonic acid (PFSA) ionomer, Nafion®, has been the benchmark of PFSA ionomer membrane due to its superior chemical and mechanical properties. Nafion® membrane, however, still suffers from poor proton conductivity at low relative humidity and high temperatures. Short side chain (SSC) PFSA ionomer has the potential to replace Nafion® due to its higher degree of crystallinity, and higher glass transition temperature, which confers better fuel cell performance.[50-51] However, the amount of research based on SSC PFSA membrane reported in the literature is still comparatively scarce.[26-27, 36-37, 52] The knowledge and

understanding of proton transport in proton exchange membrane (PEM) materials is of essential importance for the design and operation of PEM fuel cells, and a fundamental understanding of proton transport is a key factor for enhancing the fuel cell performance. Additionally, this understanding will provide valuable information about the effect of various parameters such as membrane structure and water content on the proton transport through PEM. For this reason, the objective of this research is to provide a systematic insight into the relationship between SSC polymer structure and proton transport properties.

After a brief introduction in Chapter 1, an analysis of the transport properties within a fully hydrated proton exchange membrane (PEM) at room temperature is presented in Chapter 2. The effect of ion exchange capacity (IEC) (IEC= 1000/ EW) on the water sorption properties of SSC PFSA ionomer membranes is studied by comparing membranes with different IECs. SSC PFSA ionomer membranes possessing 1.3, 1.4, and 1.5 mmol g^{-1} IEC are compared to a series of long side chain (LSC) PFSA ionomer membranes ranging in IEC from 0.9 to 1.13 mmol g^{-1}. The relationships between water content, proton conductivity, acid concentration, and proton mobility are investigated. In addition, complementary measurements of water permeability and oxygen diffusion were performed on SSC PFSA ionomer membranes and Nafion® NR211 membrane to confirm the results obtained from proton mobility.

Chapter 3 is a proposal for future studies based on the findings of this research.

2. Disorganized proton channel in short side chain PFSA ionomer membranes

2.1. Introduction

Short side chain (SSC) perfluorosulfonic acid (PFSA) ionomer possess many promising properties over long side chain (LSC) PFSA ionomer.[25-27] An increasing number of studies describing the properties of SSC PFSA ionomer membranes have been reported.[27, 53-56] Kreuer and co-workers[37]studied Dow 840 (840 g mol^{-1}) and Dow 1150, reporting that SSC PFSA membranes displayed similar water and proton transport and similar hydrophobic/hydrophilic separation as a function of water volume fraction in comparison to Nafion® 117 at a given ion exchange capacity (IEC= 1000/ EW).

The connectivity of the hydrophilic channels was reported to be reduced due to the reduced flexibility of the short side-chain architecture. Gorri et al.[57] explored water and methanol permeation through SSC Hyflon® 860 (Equivalent weight (EW) =860 g mol^{-1}) membranes and reported that water and methanol fluxes increase with temperature.

---

*Sections of this work have been reproduced by permission of the Royal Society of Chemistry: *Physical Chemistry Chemical Physics,* X. Luo, S. Holdcroft, A. Mani, Y. Zhang and Z. Shi, 2011,13, 18055-18062© 2011, RSC Publishing

Oxygen permeation data for SSC-1.3 and NR211 used in this work were obtained by Dr. Ana Mani.

De Angelis et al. studied the effect of temperature on water sorption and diffusion in a SSC PFSA membrane (EW=860 g mol^{-1}) and demonstrated that water diffusivity reaches a maximum value when the water content approaches maximum values of hydration of -SO_3H groups.[58] SSC ionomers have also been the subject of several theoretical and molecular-level modelling studies, [59-65] from which, the effects of backbone flexibility, length of side chain, IEC, and molecular weight on proton transport processes, under varying levels of hydration, have been revealed.

Compared to long side chain (LSC) PFSA analogues, the shorter side chain should allow for a much greater IEC without causing excessive swelling or dissolution, This is because the main chain sequence length between side chains will, on average, be longer for a given IEC, and hence potentially greater extent of main chain crystallization. However, reported studies of high IEC SSC PFSA ionomer membranes are relatively few. Moore and Martin[36] studied the Na^+-form of Dow's PFSA ionomer membranes (EW= 635, 803, 909, 1076 and 1269 g mol^{-1}) using WAXS. The study revealed that high IEC SSC membranes possessed a lower crystallinity index than low IEC analogues. DSC analysis revealed that Dow 635 membrane possessed endotherms due to a glass transition and a thermal transition involving ionic clusters. Compared to high EW Dow membranes, the 635 EW membrane exhibited a higher ionic cluster glass transition temperature. Also, high IEC membranes absorbed more water and possess larger ionic clusters than low IEC membranes. It was also reported that the Dow 635 Na^+-form membrane absorbs up to 80% water due to the formation of an interconnected rod-like network.[52] Ghielmi et al. examined water uptake of extruded Hyflon 670 (IEC=1.49 mmolg^{-1}) and 770 (IEC=1.30 mmolg^{-1}) membranes at 100°C.[26] Much larger

water uptakes were observed compared to low ion exchange capacity (IEC) Hyflon membranes, and molecular modelling studies of proton transport in SSC PFSA membranes (IEC=1.72 mmol g^{-1}) revealed that the calculated hydronium ion diffusion coefficient increased with water content.[65]

Noteworthy, the studies referred to above describe properties of short side chain (SSC) PFSA ionomer membranes prepared by extrusion; the properties of solution-cast SSC PFSA membranes is sparse, despite the significant effect processing conditions exert on membrane properties, as clearly demonstrated for LSC PFSA ionomer membranes.[22] Recently, Peron et al reported fuel cell performances of membrane-electrode-assemblies using high IEC SSC ionomer (1.3, 1.4, 1.5 mmol g^{-1}) as the proton conducting medium dispersed in the catalyst layer.[50] The incorporation of high IEC SSC ionomer provided improved fuel cell polarization performance at elevated temperature and under lower relative humidity.

In this chapter, attention is turned to understanding the physico-chemical and transport properties of high IEC SSC ionomer membranes. The examination was taken on the effect of IEC on water sorption, proton conductivity, and proton mobility.[47] Due to the anomalous and unpredicted properties observed, molecular transport properties were further examined using: hydraulic permeability, in the case of water transport, according to the previously developed methodology;[66] and electrochemical oxygen reduction in a solid state electrochemical cell, in order to determine oxygen diffusion.[67] The properties of SSC membranes were compared to LSC PFSA membranes possessing varying IEC in order that similarities and deviations between the two can be elucidated.

2.2. Experimental

2.2.1. Materials

Two series of as-received PFSA membranes were used in this research. These are short side chain (SSC) PFSA and long side chain (LSC) PFSA. Nafion® NR211 was used for comparative purpose. All membranes were used in their H^+-form.

SSC PFSA membranes (20 μm thick), solution-cast from dimethylformamide (DMF), provided by Shandong Dongyue Chemical Co. Ltd, were synthesized using a previously described route from $CF_2CF(OCF_2CF_2SO_2F)$ monomer.[68] SSC PFSA ionomers possessed the following ion exchange capacities (IECs) (EW): 1.3 (770), 1.4 (715) and 1.5 mmol g^{-1}(670 g mol^{-1}). These were abbreviated: SSC-1.3, SSC-1.4, and SSC-1.5, respectively.

LSC PFSA membranes (~19 μm thick) were provided by Shandong Dongyue Chemical Co. Ltd. The membranes were also cast from DMF solutions.LSC PFSA ionomers possessed the following IECs (EW): 0.94(1063), 1.05(954), 1.06(943), 1.09(917), 1.13 mmol g^{-1} (885 g $mmol^{-1}$). These were abbreviated: LSC-0.94, LSC-1.05, LSC-1.06, LSC-1.09, and LSC-1.13. NR211 (25 μm thick) was purchased from Aldrich.

Sulfuric acid and sodium chloride (99%, reagent grade) were purchased from Alfa Aesar and used as-received. Hydrogen peroxide and sodium hydroxide were purchased from Sigma Aldrich and used as-received. Milli-Q water (Millipore) was used for washing and hydrating membranes.

Membranes were first boiled in 3 vol% H_2O_2 solution for 1h, and washed with Millipore water for an hour, during which time the water was refreshed several times. Membranes were subsequently boiled in 1 M H_2SO_4 for 1h. Finally, membranes were boiled in Millipore deionized water for 1h and washed repeatedly in fresh water until the pH of the water remained constant. Membranes were stored in Millipore deionized water overnight prior to use.

2.2.2. Ion exchange capacity

Ion exchange capacity (IEC) was determined by acid-base titration. Samples (~ 10 x 20 mm) were cut from fully hydrated membranes after pre-treatment and equilibrated in 2M NaCl overnight at room temperature prior to use. The protons released were neutralized using a 0.001M NaOH to a phenolphthalein end point. Membranes were removed from sample vials after titration, washed with Millipore water several times and submerged in 0.5 M H_2SO_4 solution overnight to re-protonate. Membranes were then removed from H_2SO_4 solution followed by Millipore water washing for several times. Membranes were dried in the vacuum oven overnight and then cooled down in a dessicator. Dry sample mass was obtained using an analytical balance. Three replicates were preformed. IEC was calculated according to the following equation

$$IEC\left(mmol\ g^{-1}\right) = \frac{(V_{NaOH},mL)\times(M_{NaOH},M)}{(W_{dry},g)} \qquad \textit{Equation 2-1}$$

where V_{NaOH} and M_{NaOH} are the volume and concentration of NaOH respectively. W_{dry} is the dry sample mass.

2.2.3. Water sorption and dry polymer density

The water content of a PEM is commonly described in terms of water uptake which was determined using equation 2-2.

$$\boldsymbol{Water\ uptake} = \frac{\boldsymbol{W_{wet} - W_{dry}}}{\boldsymbol{W_{dry}}} \qquad \textit{Equation 2-2}$$

where W_{wet} and W_{dry} are the 'wet' and 'dry' weight of the membrane, respectively. Membranes were cut into rectangular pieces and equilibrated in Millipore water overnight at room temperature prior to use. At least three replicates were performed. 'Wet' membranes were equilibrated in Millipore deionized water overnight at room temperature, and surface water removed and wet weights were obtained. This was carried out quickly (< 30 s) to avoid water loss from the membrane. Dry weights were obtained after vacuum drying to a constant weight at 80 °C overnight and cooled in a desiccator. This was performed within 30 s to avoid the absorption of water vapour from the atmosphere.

Water uptake as a volume percentage was also calculated as X_v. This is a more useful measurement, as it represents the actual volume fraction of water in the membrane. X_v was estimated using equation 2-3

$$\boldsymbol{X_v} = \frac{\boldsymbol{V_{water}}}{\boldsymbol{V_{wet}}} \qquad \textit{Equation 2-3}$$

where V_{water} is the volume of water contained in the membrane; and V_{wet}, is the total volume of the wet membrane. To obtain V_{water}, the mass of free water in the membrane and its density (1.0 g cm^{-3}) were used. In order to estimate V_{wet}, a digital micrometer (±0.001mm, Mitutoyo) was used to obtain the thickness and a digital calliper (±0.1mm, Mitutoyo) was used to obtain the width and length of the membrane.

Another key parameter describing water sorption is λ, which represents the number of water molecules that are contained in the membrane per acid group (-SO_3H). A schematic diagram representing λ of the membrane is shown in Figure 2.1. Equation 2.4 was used for calculating λ.

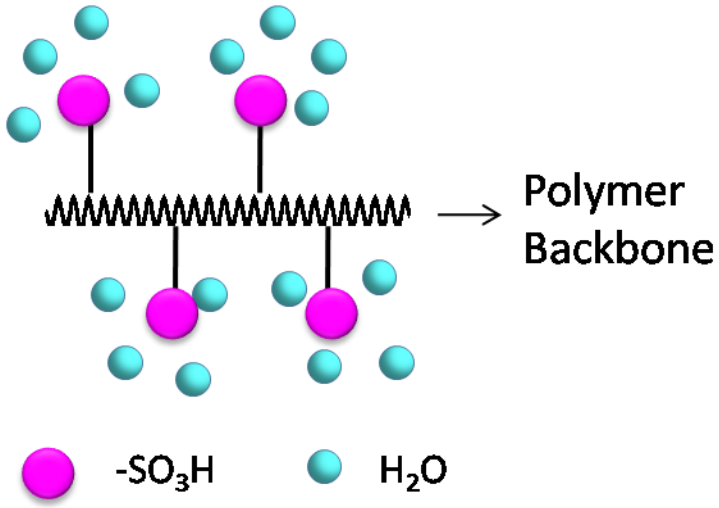

Figure 2.1 Schematic illustration of λ= 4

$$\lambda = \frac{water\ uptake\ (\%) \times 10}{18 \times IEC\ (mmol\ g^{-1})} \qquad \textit{Equation 2-4}$$

Polymer dry density The polymer dry density (ρ) was calculated using the following equation,

$$\rho = \frac{W_{dry}}{V_{wet} - V_{H_2O}} \qquad \textit{Equation 2-5}$$

where W_{dry} is the weight of dry sample, V_{wet} is the volume of the wet sample, and V_{H2O} is the volume of water in the wet membrane.

2.2.4. *Proton conductivity*

Proton conductivity was measured using electrochemical impedance spectroscopy (EIS) with a Solartron 1260 frequency response analyzer (FRA), employing an in-plane, two-electrode configuration (Figure 2.2 left). A strip of rectangular, fully hydrated membrane (Figure 2.2 right) was contacted by two Pt electrodes, and an alternating current was passed along the plane of the sample. Two wires fitted with alligator clips connected the probe to the FRA, and Nyquist plots (Figure 2.3) between 100 MHz-100Hz were obtained. This cell assembly was wrapped with a piece of plastic film to keep the samples from losing water to atmosphere before completion of the measurement. Membrane resistances were extrapolated by fitting the data to the standard Randles equivalent circuit (Figure 2.4).

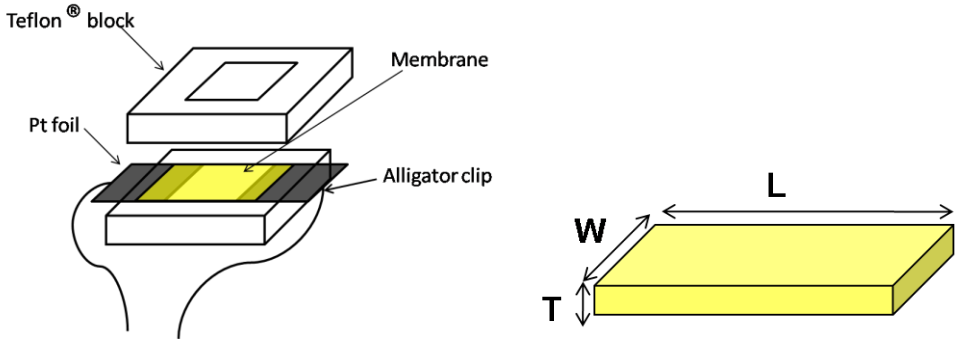

Figure 2.2 Schematic diagram of proton conductivity measurement (left) and rectangular PEM sample dimensions (right).

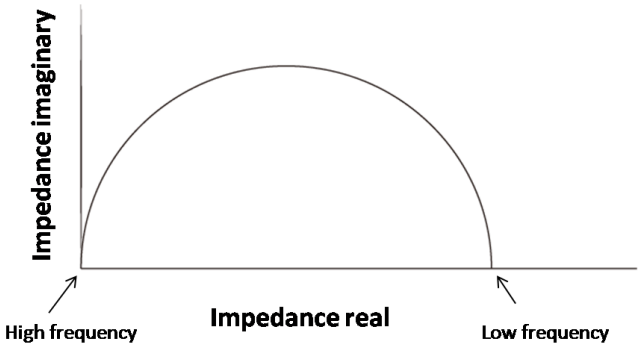

Figure 2.3 The schematic diagram of Nyquist plots

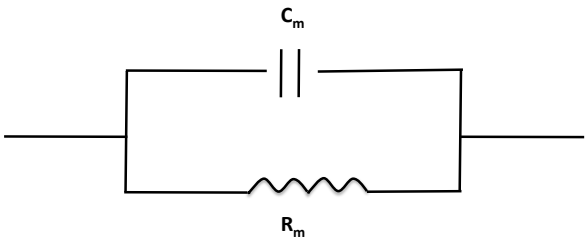

Figure 2.4 A simple schematic diagram of Randles-type equivalent circuit

Proton conductivity was calculated using equation2-6:

$$\sigma_{H^+} = \frac{L}{R\,A} \qquad \textit{Equation 2-6}$$

where *L* (cm) is the distance between electrodes, *R* (Ω) is the ionic resistance of the membrane determined from the AC impedance spectra. *A* (cm^2) is the cross sectional area of the sample. The thickness was obtained using a digital micrometer (±0.001mm, Mitutoyo). The length and width were obtained using a digital calliper

(±0.1mm, Mitutoyo). The resistivities of the membranes were calculated using Zplot 2.8 software (Scribner Associates, Inc.).

2.2.5. Acid concentration and effective proton mobility

Acid concentration The acid concentration represents the overall free proton concentrations in the membrane, which was determined using equation 2-7.

$$[-\boldsymbol{SO_3H}] = \frac{\boldsymbol{W_{dry}\,(g)}}{\boldsymbol{V_{wet}(cm^3)}} \times \boldsymbol{IEC}\ (\boldsymbol{mmol\ g^{-1}}) \qquad \textit{Equation 2-7}$$

where W_{dry} is the dry weight of membrane and V_{wet} is the wet volume of membrane.

Effective proton mobility The effective proton mobility (μ'_{H+}) was determined using equation 2-8.

$$\boldsymbol{\mu'_{H^+}} = \frac{\boldsymbol{\sigma_{H^+}}}{\boldsymbol{F}\,[-\boldsymbol{SO_3H}]} \qquad \textit{Equation 2-8}$$

where F is the faraday constant. σ_{H+} is the proton conductivity of the membrane. [$-SO_3H$] is the acid concentration of the membrane.

2.2.6. Hydraulic permeability

A schematic diagram of setup is shown in Figure 2.5. A syringe (Gastight® #1025, Hamilton Co. with PHD 2000, Harvard Apparatus) filled with deionized water, a mass flow meter (2.0 µL/min µ-FLOW, Bronkhorst HI-TEC) and a pressure transducer (PX302.100GV, Omega Engineering Inc.) were connected in series with "1/8" OD polytetrafluoroethylene (PTFE) tubing. The membrane was placed in a cell consisting of a PTFE coated stainless steel screen and an O-ring. The area of membrane was 3.66 $\times 10^{-4}$ m^2.The cell was operated at 24 (±1) °C. Measurements were taken in the constant flow rate mode when the pressure had equilibrated. The apparatus was controlled and monitored using Lab view® software. For hydraulic permeability measurements only, the thicknesses of the SSC ionomer membranes were > 20 µm, and are listed in the results section.

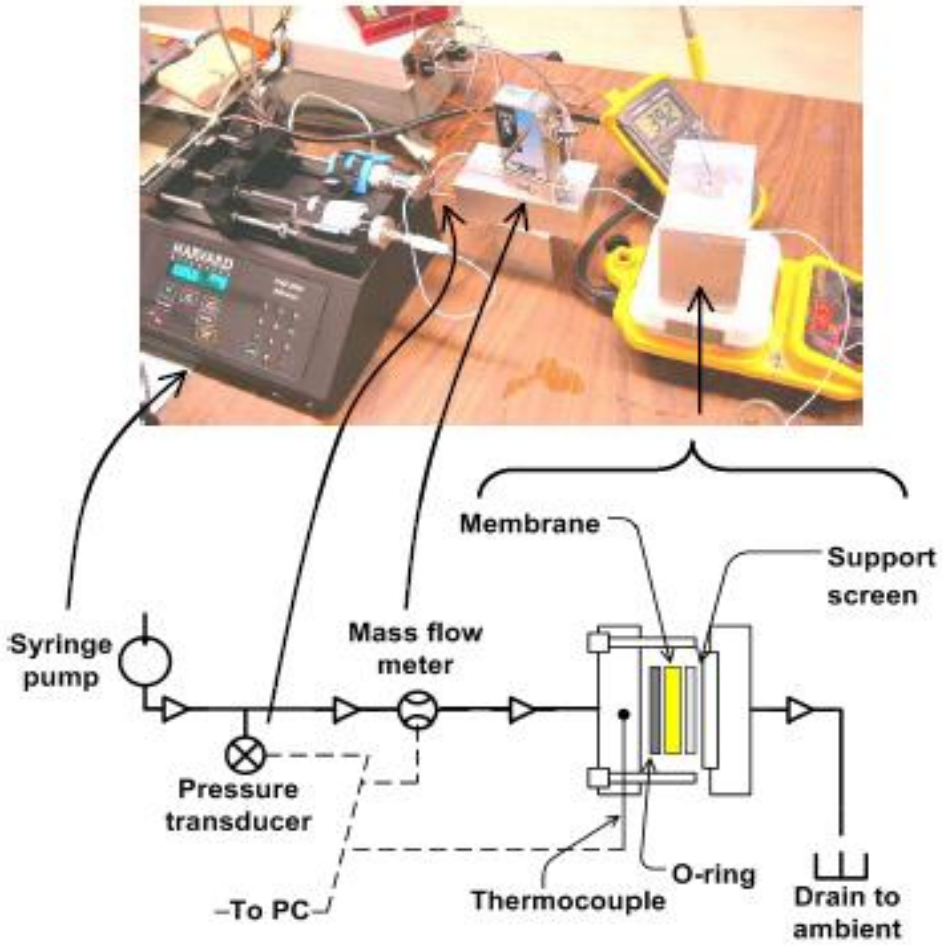

Figure 2.5 Photograph and schematic of liquid-liquid permeation (LLP) setup. Syringe, mass flow meter, and the pressure transducer were placed at room temperature.

(Reprinted from ref. [66] with the permission of The Electrochemical Society©2009.)

2.2.7. Oxygen diffusion

Oxygen diffusion was measured using solid-state electrochemical cell methodology[69-72] by Dr. Ana Mani. The solid polymer electrolyte membrane was sandwiched between a 50 µm radius Pt micro-disc working electrode (WE), Sandfire

Scientific Ltd., Gibsons, Canada, diametrically opposed to a 0.25 mm diam. Pt wire of a dynamic hydrogen electrode (DHE) and a Pt gauze counter electrode (CE). The assembly was housed in a home-built environmental chamber. Prior to electrochemical analysis, the electrodes were polished with 0.05 micron alumina. In order to increase the surface area of the Pt micro-disc, the electrode was platinized by potential cycling (1.2 V to -0.2 V) in 1 mM K_2PtCl_6 in 0.5 M H_2SO_4 solution at 50 mV/s scan rate for ~5 hours. The electrochemical response of the working electrode was examined in N_2 saturated 0.5 M H_2SO_4 versus a saturated calomel electrode (SCE). The electrochemical surface area (ESA) was estimated using the charge under the hydrogen adsorption region of a voltammogram using 210 $\mu C\ cm^{-2}$ as the conversion factor for charge-to-area.[73] The geometric area was $7.854\times10^{-5}\ cm^2$ and the roughness factor was 2.5.

Cyclic voltammograms (CVs) were recorded using an EG&G PARC Model 283 potentiostat. The oxygen pressure inside the chamber was 30 psi, the relative humidity (RH) was 100% and the temperature was 30 °C. The electrode was scanned for 100 cycles between 1.4 and 0.1 V at 100 mV/s to clean the Pt | membrane interface prior to measurements. Chronoamperometry (CA) was carried out by holding the potential of the Pt micro-disc at 1.2 V for 20 seconds and then stepping to 0.4 V for 10 seconds. Values of D_{O2} were obtained from the average of five chronoamperometric trials according to published procedures.[69, 71]

2.3. Results and discussion

2.3.1. Water sorption

The IEC of a membrane has a strong effect on the amount of water absorbed. Generally, the greater the number of the hydrophilic sites, the more water is absorbed. Water volume content, X_v, and number of water molecules per sulfonic acid group, λ, of fully hydrated SSC PFSA membranes at ~25°C are shown in Figure 2.6. Despite the fact that only 3 membranes of different ion exchange capacity (IEC) were available for analysis, the water contents are observed to increase with IEC, both in terms of X_v and λ. X_v for SSC membranes is 2 to 4 times larger than for LSC membranes, which increases with IEC. The water volume contents for the SSC membranes (56 to 75%) are much larger than for NR211 (26%). λ for SSC-1.3 (~15) is similar to that exhibited by LSC membranes that possess much smaller IECs (0.9-1.13 mmol g^{-1}) but slightly larger than NR211 (~13). The increasing λ with IEC for the SSC membranes falls on a lower trend line than that for LSC membranes, indicating that water sorption is slightly suppressed in SSC membranes. SSC membranes exhibit much higher water content, X_v, than LSC membranes but possess relatively similar λ values – as illustrated in a plot of λ against X_v (Figure 2.7). This is due to the SSC membranes possessing a greater dry polymer density as shown in Figure 2.8. Plots of λ against X_v often reveal insights into membrane swelling phenomena: for example, λ may remain unchanged over a wide range of X_v, increase steadily with X_v, or may increase dramatically at a given water volume.[47] In the present case, based on the observed trends for SSC and LSC, SSC swells less than LSC.

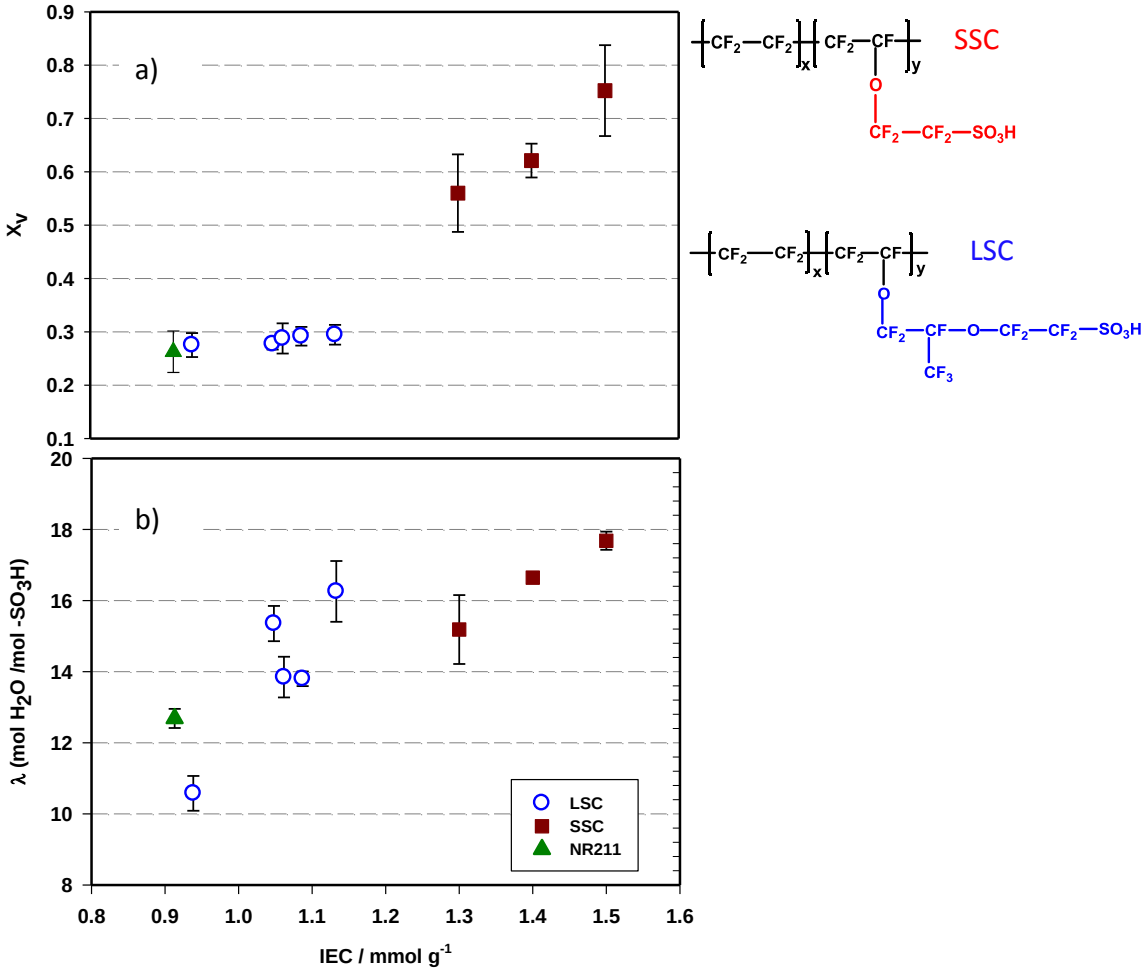

Figure 2.6 Water content (X_v(a) and λ (b)) of fully hydrated SSC PFSA, LSC PFSA and NR 211membranes, as a function of IEC at ~25 °C.

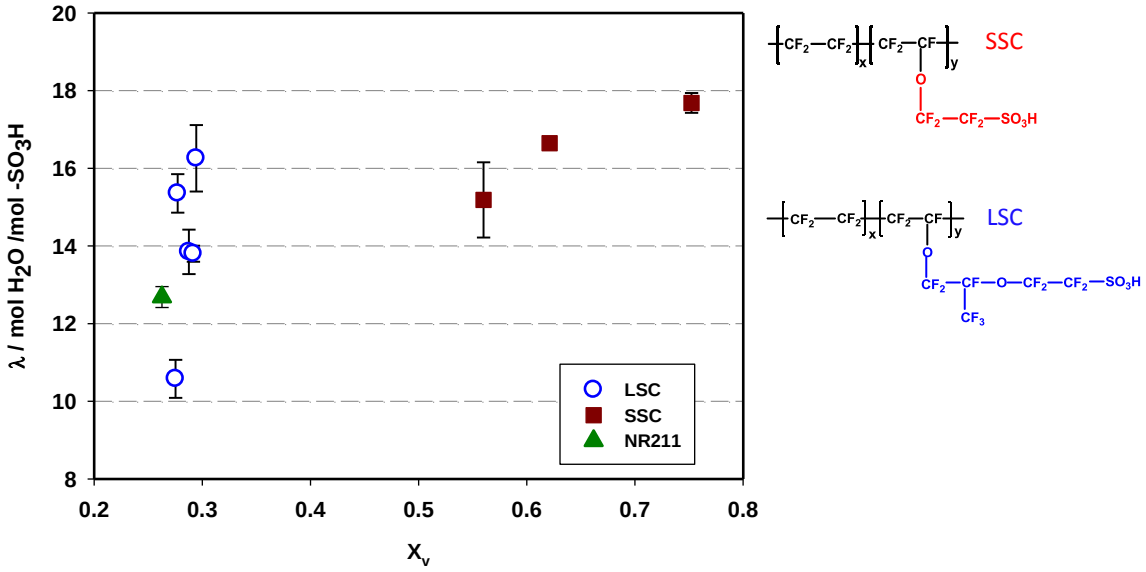

Figure 2.7 λ of SSC, LSC and NR211 membranes as a function of X_v at ~25 °C

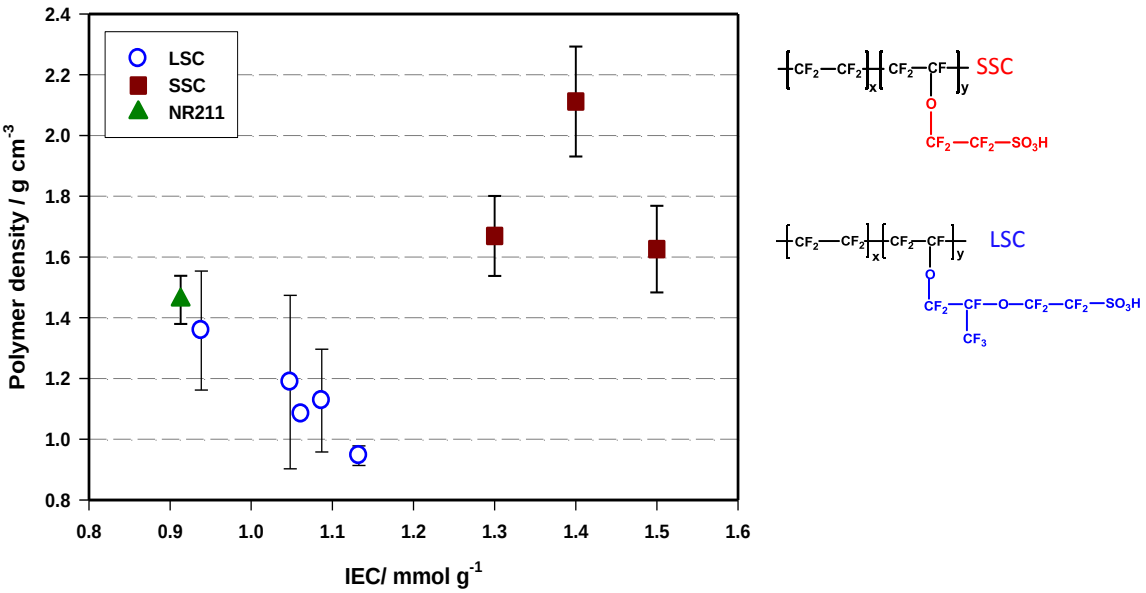

Figure 2.8 Dry density of PFSA membranes as a function of IEC at ~25 °C

2.3.2. *Proton conductivity and acid concentration*

The proton conductivity of the 3 fully-hydrated SSC PFSA membranes at ~25 °C ranged between 88 and 115 mS/cm as shown in Figure 2.9. No obvious trend exists between conductivity and IEC within this series. In contrast, the proton conductivity of LSC PFSA membranes increases with increasing IEC, consistent with reports for Nafion®-based membranes. A commercial sample of Nafion®-NR211 falls on the trend line for the LSC membranes. The SSC PFSA membranes exhibit higher conductivity than NR211 and exhibit similar values to LSC membranes having IECs 0.9 to 1.13 mmol g^{-1}. However, it is clear the SSC membranes do not scale in proton conductivity as a function of IEC according to the trend observed for the LSC membranes – that is, the SSC membranes possessed much lower proton conductivity than anticipated, given their high IEC.

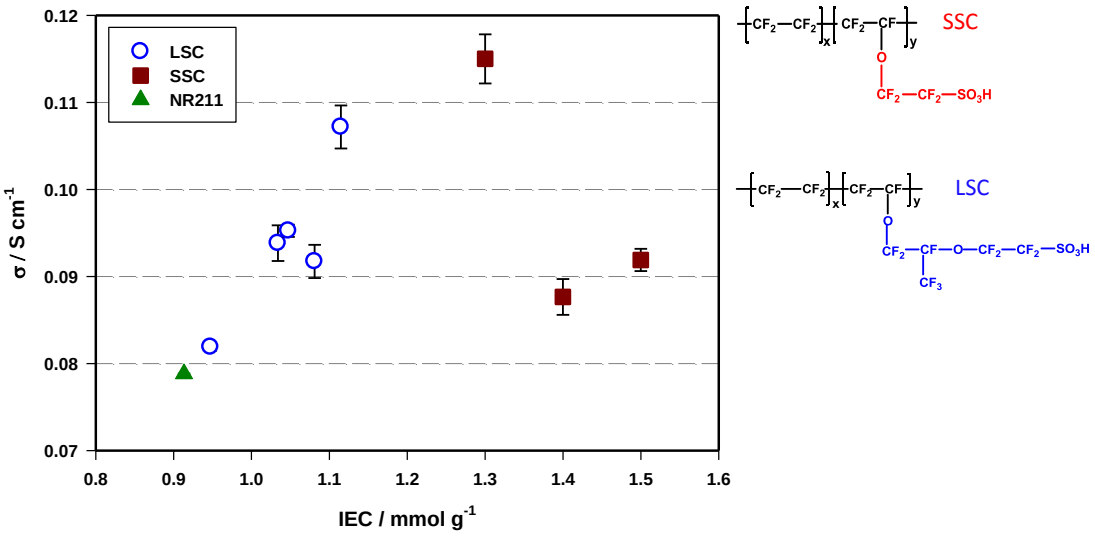

Figure 2.9 Proton conductivity of fully hydrated SSC PFSA, LSC PFSA and NR211 membranes as a function of IEC at ~25 °C.

The relationship between conductivity and water content was investigated because hydrated protons travel through the aqueous phase of the ionomer membrane. A plot of conductivity as a function of water content (X_v) is plotted in Figure 2.10. A remarkable feature is that despite the water contents (X_v) of SSC membranes being 2 to 2.5 times larger than LSC membranes, and despite proton conduction being very dependent on water volume - as illustrated by the large increase in conductivity with small changes in water contents for the LSC membranes series - the SSC membranes only exhibit conductivities similar to the highest IEC LSC membranes. Often, high IEC membranes possess low proton conductivities due to excessive sorption of water and reduced proton concentration. However, as illustrated in Figure 2.11, the analytical acid concentrations [$-SO_3H$] are ~ twice as large for SSC membranes (2.3 M) as they are for the LSC analogues (1-1.5 M). Thus, as shown in Figure 2.6 not only is the water volume in SSC membranes twice as large as in LSC membranes, so too is [$-SO_3H$]. Collectively, these two parameters should impart much higher proton conductivity to the SSC membranes than is observed. This observation is consistent with a report by Kreuer et al.[37] using small angle X-ray diffraction spectra that states there is less pronounced separation of hydrophilic and hydrophobic domains in Dow SSC PFSA (EW=858 g mol^{-1}) membrane, resulting in a lower than anticipated proton conductivity.

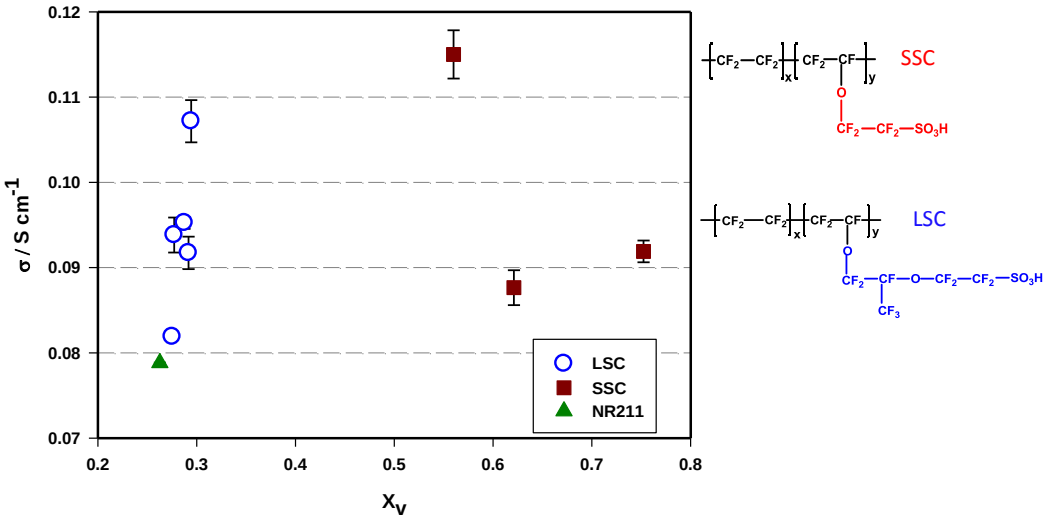

Figure 2.10 Proton conductivity of fully-hydrated PFSA membranes as a function of X_v at 25°C.

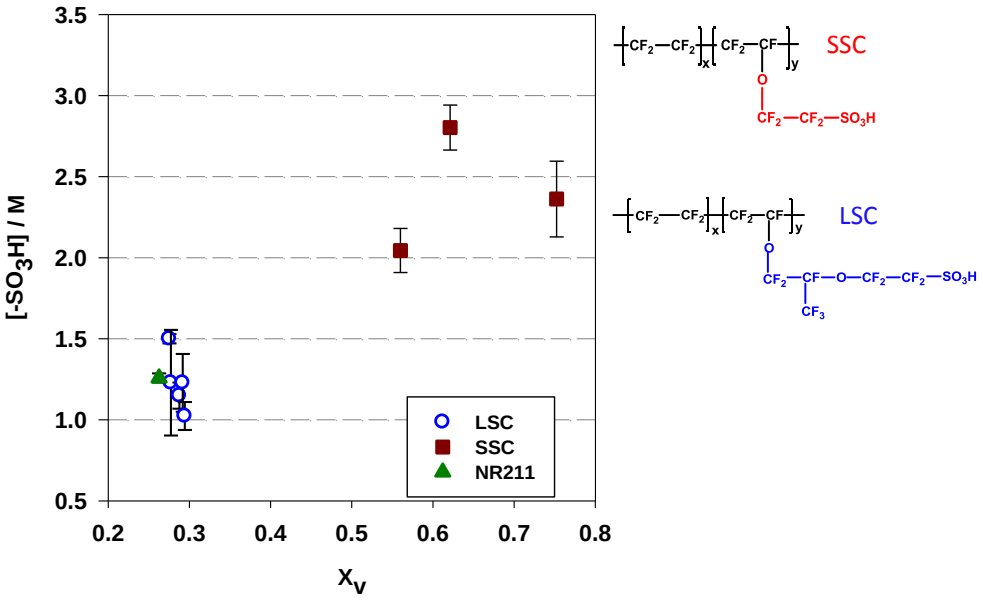

Figure 2.11 [-SO_3H] of fully hydrated PFSA membranes as a function of X_v at ~25 °C

2.3.3. *Effective proton mobility*

From measured proton conductivities and calculated values of [-SO_3H], the effective proton mobility, μ'_{H+}, was estimated, which provides information on the combined influence of the tortuosity of the hydrophilic pathways and dissociation of the proton and pendent sulfonate anion. Both are strongly influenced by water content. Plots of μ'_{H+} vs. X_v and vs. IEC are shown in Figure 2.12 and a plot of μ'_{H+} vs. λ is shown in Figure 2.13. The proton mobility in SSC membranes is similar in range to NR211, even though SSC membranes relatively contain much more water (56 -75 vol% compared to ~25 vol% for NR211). λ values are similar (SSC ~15, NR211 ~13). Moreover, the proton mobilities are much lower than the highest IEC LSC membranes despite the fact that SSC membranes exhibit relatively similar λ values and much higher water contents. Thus proton mobility in SSC membranes is observed to be much lower than expected compared to LSC membranes despite the larger fraction of hydrophilic domains that SSC membranes possess. In relation to this, theoretical modelling indicates that the minimum number of water molecules required to effect proton transfer increases with an increase in the number of tetrafluoroethylene (TFE) units in the backbone that separate two juxta-positioned side chains.[74] In the case of SSC ionomer, for a given IEC there are more TFE units that separate the nearest two side chains than in the case of LSC ionomer. Thus a higher λ value is needed to effect proton transport in SSC membranes. The experimental data (shown in Figure 2.13) reveals that SSC membranes do not possess much higher λ values than LSC analogues, even though IECs are higher, thus proton mobilities are lower than anticipated, which is consistent with the prediction made through modelling studies.

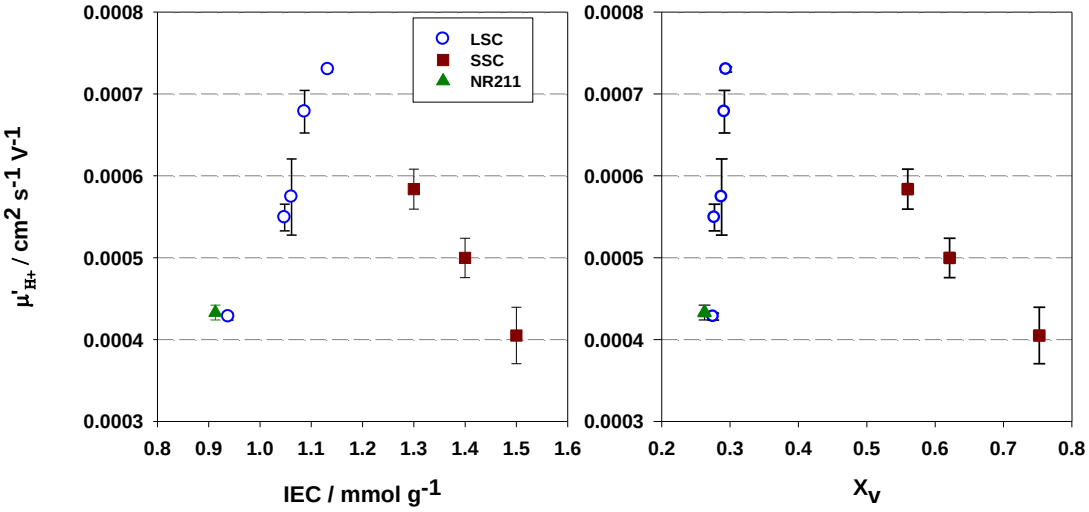

Figure 2.12 Effective proton mobility, calculated according to Eq.2.8, for PFSA ionomer membranes at ~25 ˚C

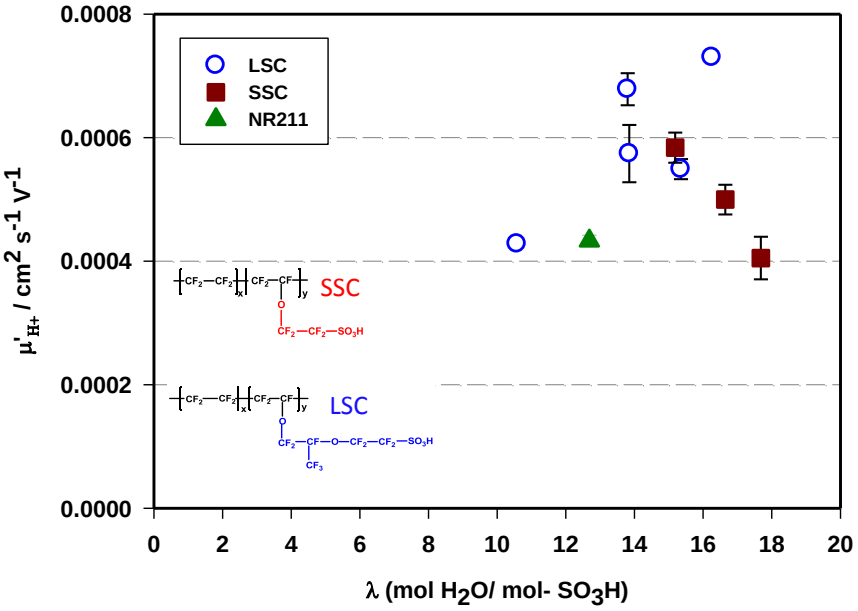

Figure 2.13 Proton mobility of PFSA membranes as a function of λ at ~25 ˚C

2.3.4. Water permeation

Hydraulic permeability was determined for liquid-equilibrated membranes wherein a pressure gradient of liquid water was forced across the experiment cell. Water permeation using liquid-liquid interfaces rather than other methods available, such as vapour-vapour permeation (VVP) and liquid-vapour permeation (LVP), was chosen because liquid-liquid interfaces reduce the influence of water vapour adsorption and desorption processes on the overall permeation of water. Thus, hydraulic permeability provides direct information on the mobility of water within the membrane, and circumvents complications caused by interfacial water transport.[66]

Water transport through selected membranes was measured under the influence of hydraulic pressure. The hydraulic fluxes of water through SSC membranes are shown in Figure 2.14. Each data point represents the steady state flux at a given pressure difference. The slope of the plot, the permeance, decreases in gradient across the series SSC-1.3 to SSC-1.4 to SSC-1.5. The permeability which is calculated by water permeance normalized to membrane thickness, are summarized in Table 2.1.

Table 2.1 Hydraulic permeability of SSC PFSA and NR211 at ~25 ˚C

PEM	Thickness (μm)	Water Content (Vol %)	Permeability ($m^2Pa^{-1}s^{-1}$)
SSC-1.3	160	56	2.28E-17
SSC-1.4	195	62	2.08E-17
SSC-1.5	98	75	3.50E-18
NR211	25	26	8.00E-18

As can be seen in Table 2.1, the permeability of the SSC membranes decreases with IEC increasing. The permeability of SSC-1.5 is almost an order of magnitude smaller than SSC-1.3 and SSC-1.4. Moreover, much higher pressures were required to achieve the desired flow rate in SSC-1.5 (Figure 2.14). The permeabilities of SSC-1.3 (2.28×10^{-17} m^2 Pa^{-1} s^{-1}) and SSC-1.4 (2.08×10^{-17} m^2 Pa^{-1} s^{-1}), are larger than NR211 but not as large as expected given their high water content. Moreover, the permeability of the SSC-1.5 membrane ($3.5 \times 10^{-18} m^2$ Pa^{-1} s^{-1}) is less than half that of NR211 (8.0×10^{-18} m^2 Pa^{-1} s^{-1}). Even though the water content of SSC- 1.5 is ~3 times greater than NR211 (75 vol%, vs. 26 vol%). As in the case of the effective proton mobility, the transport of water through SSC membranes is much slower than anticipated given their higher water contents.

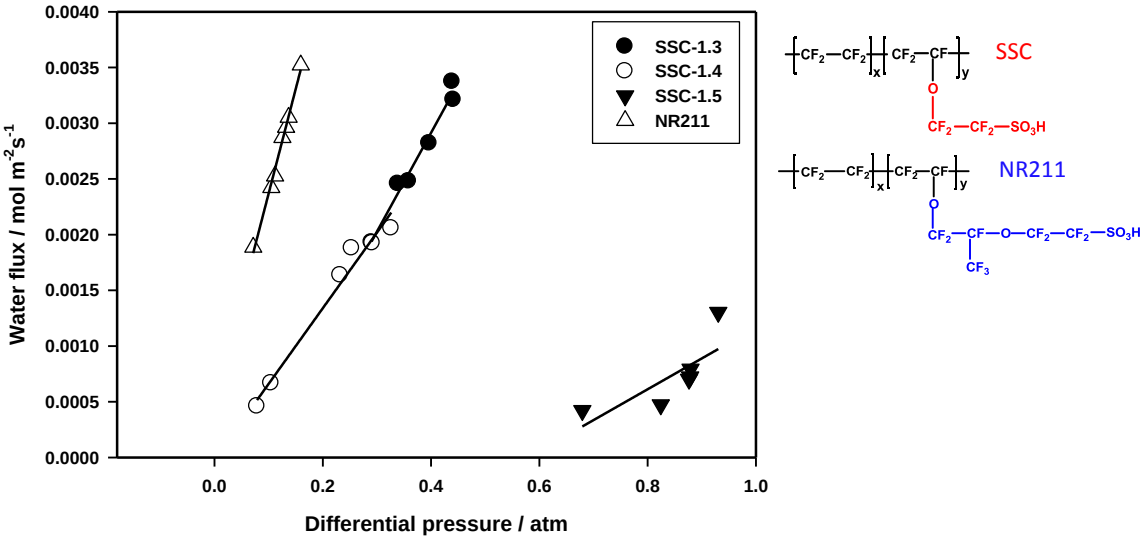

Figure 2.14 Water permeation through PFSA membranes as a function of differential hydraulic pressure at~25 °C

As hydrated protons similarly require an aqueous phase for transportation, it was useful to plot the effective proton mobility, μ'_{H+}, versus water permeability, shown in

Figure 2.15. The effective proton mobility shows a strong correlation with the measured water permeability which confirms the supposition that water and protons travel the same tortuous path.

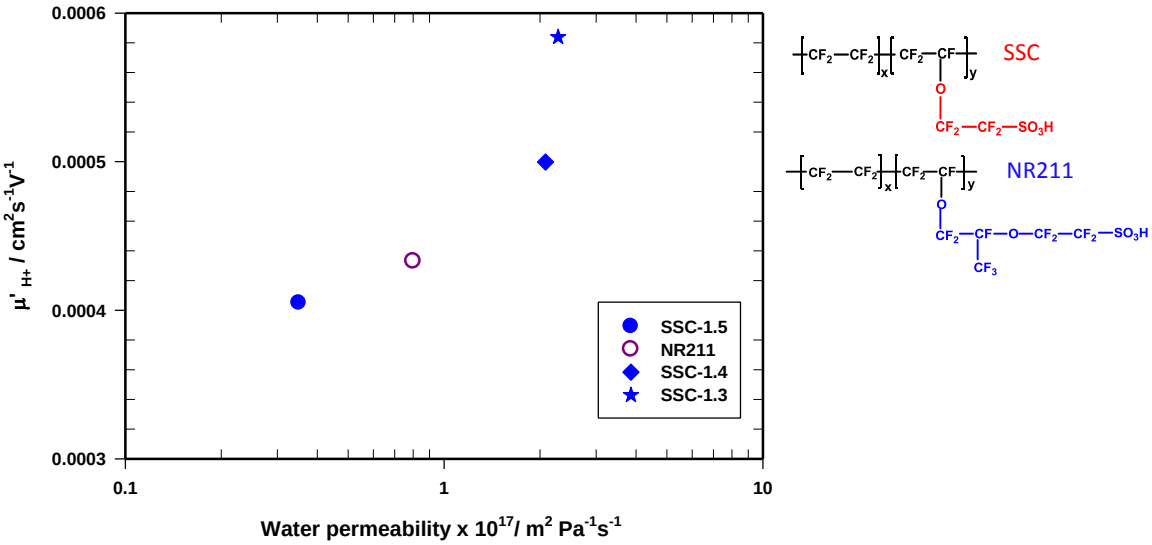

Figure 2.15 Effective proton mobility in PFSA ionomer membranes vs. water permeability at ~25 ˚C

2.3.5. Oxygen diffusion

Oxygen transport was reported to occur in the hydrophilic pathway of PEMs,[75]therefore,examination of oxygen diffusion within a PEM may provide the information of the tortuosity of proton transport pathway. Mass transport parameter associated with the oxygen reduction reaction, e.g., O_2 diffusion coefficient, in one of the SSC membranes (SSC-1.3) was determined chronoamperometrically using a solid state electrochemical cell, as described in the experimental section. In order to aid comparison with the transport properties of protons and water described above, measurements were

made at a similar temperature (30°C). The diffusion coefficient, D_{O2}, for SSC-1.3 and NR211 membranes are listed in Table 2.2.

Table 2.2 The diffusion coefficient for SSC-1.3 and NR211 at 30 °C, 100% RH and 30 psi O_2

PEM	$D_{O2}\times10^6$ ($cm^2\ s^{-1}$)
SSC-1.3	1.69±0.42
NR211	1.13±0.31

As shown in Table 2.2, SSC-1.3 membranes exhibit higher D_{O2} value compared to NR211. Similar to the observations of proton and water transport in SSC-1.3 membranes, this is not an entirely expected result, given that D_{O2} is strongly correlated to water content.[67, 75] The diffusion coefficient in the SSC-1.3 membrane are lower than anticipated given its much higher water content (56% vs. 26 vol%). In the case of previous studies of oxygen diffusion coefficient determined for other polymer membranes containing more than 50 vol% water, including sulfonated, trifluorostyrenes, block copolymers, and various graft copolymers, under similar conditions, the measured diffusion coefficients is an order of magnitude greater, commensurate with their water content.[76]

The observation that proton mobility, water permeability, and oxygen diffusion coefficient are all lower in value than anticipated leads to the conclusion that the

hydrophilic percolation network for the transport of molecular species is much less developed in SSC membranes than it is for LSC membranes, as originally indicated by Kreuer et al., although for an alternate source of SSC PFSA ionomermembrane.[9]

2.4. Summary and conclusion

In comparison to long side chain(LSC) PFSA ionomer membranes, the short side chain (SSC) membranes studied possessed a higher average ion exchange capacity (IEC) and, as a consequence, a much higher water content. The proton conductivity of high IEC, SSC PFSA membranes is greater than for NR211 membranes, and comparable to the LSC membranes examined. The dry polymer density of high IEC SSC membrane was greater than the other membranes examined, the analytical $-SO_3H$ concentration of hydrated membranes was very much higher, but the proton mobility was not as commensurately high, over the range of IEC studied.

While the water uptakes of LSC PFSA ionomer membranes correlate well with IEC, and the relative water contents (X_v) of SSC membranes were commensurately larger due to their much higher IEC, the λ values were lower than expected given the trend observed for LSC membranes. The SSC membranes possessed very high acid concentrations and much higher water contents in comparison to the LSC membranes examined, including NR211. However, this did not translate into a multi-fold increase in proton conductivity. Rather, SSC membranes were found to possess suppressed proton mobility, even though λ values were reasonably large and the water content very high. This work suggests the network of hydrophilic channels is poorly developed compared to LSC analogues. Ex- situ measurements of water permeability and oxygen diffusion, both

requiring hydrophilic channels, also support the assertion that the connectivity of the hydrophilic network is not as well developed as in LSC PFSA membranes, suggesting that the additional water volume sorbed into the high IEC SSC membranes is not fully utilized. These observations bring to mind the morphological picture of a larger than usual number of 'dead-ends' or 'necking" of channels, as illustrated in Figure 2.16, akin to Kreuer's much referenced description of the morphology of hydrocarbon membranes[22] and reiterated for Dow membranes.[37]

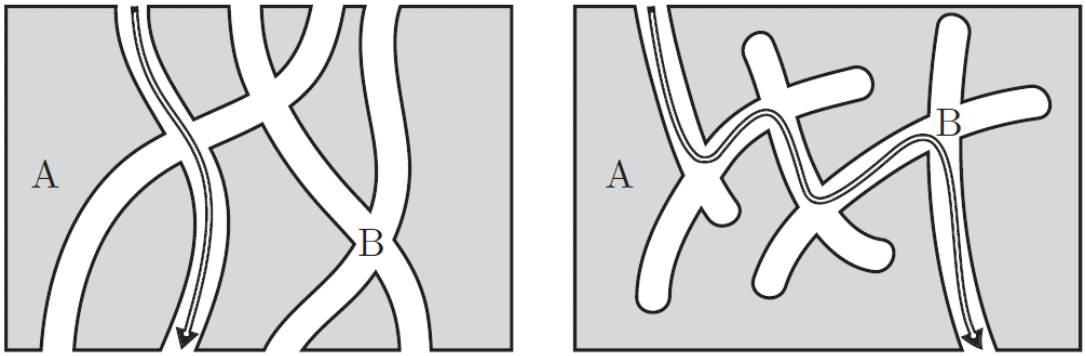

Figure 2.16 Schematic diagram illustrating the difference in proton conduction pathways for LSC PFSA (left) and SSC PFSA (right) ionomer membranes, where A represents the perfluorinated matrix; and B, the hydrophilic channels.

This work provides experimental verification of the studies of Brandell et al.[64] using molecular dynamics studies to assert that SSC-based membranes exhibit a less than ideal connectivity of water channels compared to LSC PFSA ionomer analogues, such as Nafion®. The study suggests that, should the connectivity of the hydrophilic network be improved, and tortuosity reduced, either by finer control of the ionomer structure or by adopting more favourable membrane processing conditions, then the

transport properties may be dramatically improved, and proton conductivities increased compared to current SSC PFSA ionomer membranes.

3. Future work

This thesis work reveals that proton transport properties are strongly correlated to water content, ion exchange capacity (IEC) and proton concentration. Proton transport properties of SSC membranes were studied under fully hydrated conditions which provided a simple and quick evaluation of a membrane transport abilities; however, under fuel cell operation the membranes are rarely fully hydrated. Generally, fuel cells are operated at lower relative humidities and higher temperatures. An adequate water content of the membrane is essential to maintain good proton conductivity and satisfactory fuel cell performance. If the hydration level is too low, bulk water is lost from the membrane and hence the membrane's proton conductivity drops.[47] Increasing the operating temperature improves the kinetics of the oxygen reduction reaction that occurs at the electrode,[1, 23] and can simplify thermal and water management of the system.[77] But if the temperature is too high, the membrane dehydrates and proton conductivity and fuel cell performance are reduced. Loss of water by the membrane at elevated temperature can be made worse if the polymer chain rearranges to cause morphological changes in the membrane, potentially resulting in reduced membrane stability and poorer performance. Therefore, raising the polymer glass transition temperature is a strategy for developing new proton exchange membrane with improved thermal properties. Here, short side chain PFSI membranes potentially possess an inherent advantage over long side chain PFSI analogues. In the literature, SSC PFSI membranes were reported to

provide better fuel cell performance over LSC analogues under elevated temperature and low humidity conditions.[27, 29] As illustrated in Figure 3.1, the proton conductivity of Aquivion® membrane was measured at different RH values, over a wide temperature range from ambient to 120°C.The results were shown that SSC membrane obtained relatively higher proton conductivity under the condition of higher temperature and greater degree of RH.

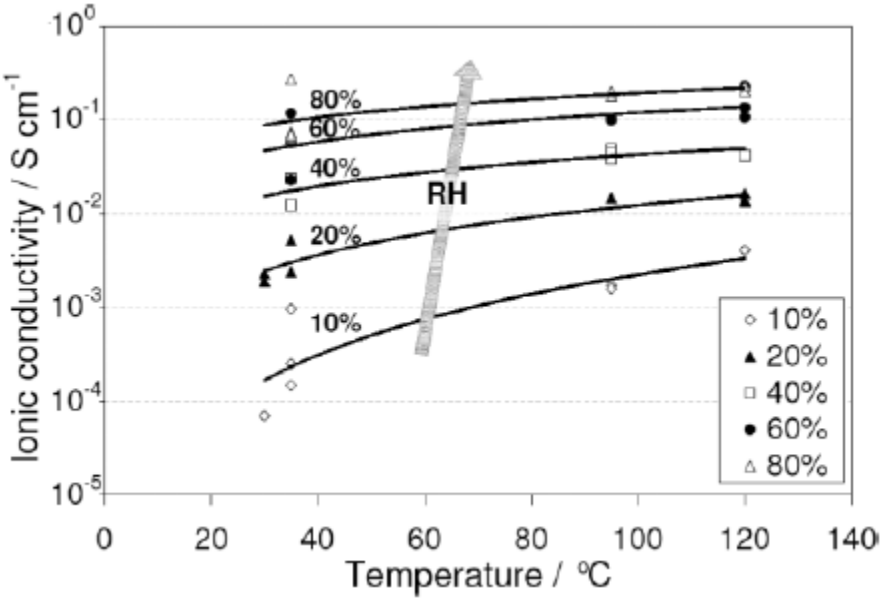

Figure 3.1 Variation of the ionic conductivity for an SSC (Aquivion®) membrane as a function of temperature at different levels of relative humidity (RH).

(Reprinted from ref.[29] with the permission of WILEY-VCH Verlag GmbH & Co. KGaA, Copyright 2010.)

To this end, in future work, proton transport properties of SSC membranes should be re-studied under controlled relative humidity (RH) and higher temperature in order to determine the effect of changing RH on water contents and membrane proton transport

properties. The study can be extended to different IEC membranes and varied measurement conditions (i.e., temperature and RH). In addition, these studies could be directly correlated with fuel cell polarization data published in the literature.[50] Water contents would require the use of dynamic gravimetric vapour sorption to determine lambda values and water volumes fraction, while proton conductivities would require specialized equipment allowing measurements to be performed under controlled environments. Such measurements would be more applicable to interpreting fuel cell data that indicated that SSC ionomer membranes offer a slight increase in performance over long side chain ionomer analogs. Preliminary results of these measurements have been obtained. A plot of proton conductivity as a function of relative humidity (RH) at 80°C is shown in Figure 3.2. An increase in RH has a dramatic effect on proton conductivity. For all the membrane series, proton conductivities increase as increasing the RH of membranes. Further examination of Figure 3.2 reveals additional information. Proton conductivity values of SSC series are significant larger than Nafion® 211 membrane given RH > 50%. In order to interpret these data, more work on these membranes is needed.

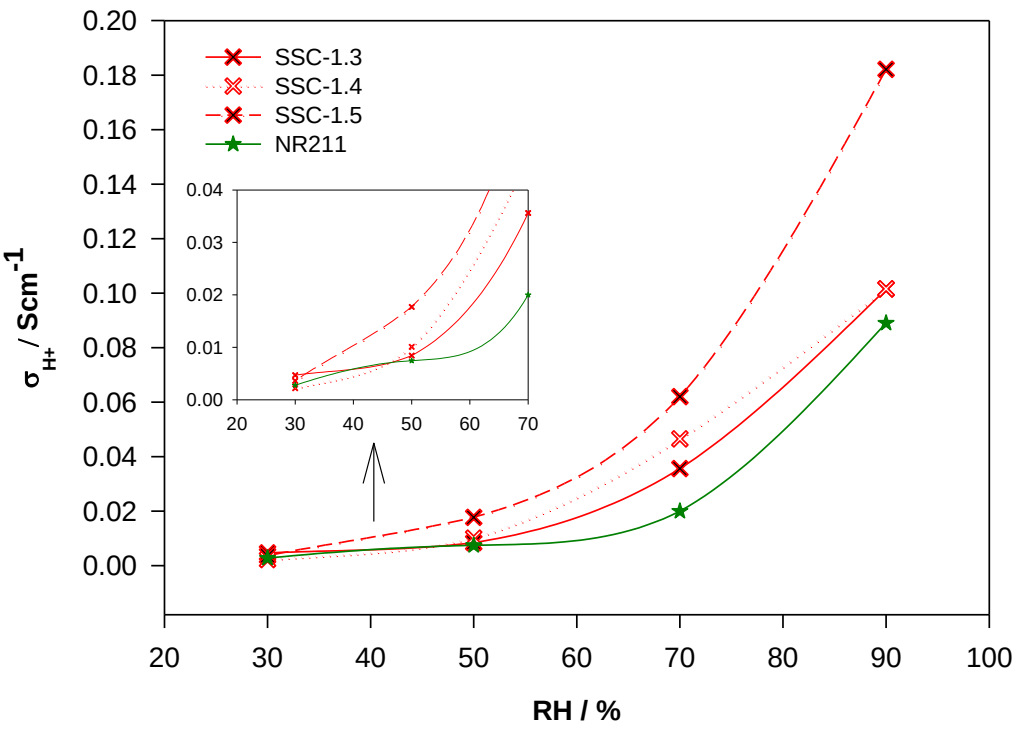

Figure 3.2 Proton conductivity of PFSA membranes as a function of relative humidity at 80 °C

As the polymer structure and morphology appear to be critical to understanding proton transport properties of membrane systems, more work is need to investigate the morphology of these membranes and its relationship to the membrane structure at various hydration level. Additionally, a deeper understanding of the structure-property relationship for these membranes at the molecular level can be obtained by study membrane morphology using transmission electron microscopy (TEM) and X-ray diffraction (XRD).

References

1. S. Bose, T. Kuila, T. X. H. Nguyen, N. H. Kim, K.-t. Lau and J. H. Lee, *Progress in Polymer Science*, 2011, **36**, 813-843.

2. O. Diat and G. Gebel, *Nature Material*, 2008, **7**, 13-14.

3. W. Reitz, *Materials and Manufacturing Processes*, 2007, **22**, 789-789.

4. C.-Y. Wang, *Chemical Reviews*, 2004, **104**, 4727-4766.

5. R. Devanathan, Energy & Environmental Science, 2008, 1, 101-119.

6. B. C. H. Steele and A. Heinzel, *Nature*, 2001, **414**, 345-352.

7. E. G. S. Parsons, *Fuel Cell Handbook*, 2000, **5**.

8. J. Appleby, R.L. Foulkes, *Fuel Cell Handbook*, NY1989.

9. C. S. Spiegel, *Designing and Building Fuel Cells*, The Mc Graw- Hill Companies, New York, 2007.

10. J. Larmine and A. Dicks, *Fuel Cell Systems Explained*, John Wiley& Sons Ltd, New York, 2003.

11. S. J. Hamrock and M. A. Yandrasits, *Journal of Macromolecular Science, Part C: Polymer Reviews*, 2006, **46**, 219-244.

12. V. M. Vishnyakov, *Vacuum*, 2006, **80**, 1053-1065.

13. Q. Ye and T. S. Zhao, *Electrochemical and Solid-State Letters*, 2005, **8**, A211-A214.

14. S. J. Hamrock and M. A. Yandrasits, *Polymer Reviews*, 2006, **46**, 219-244.

15. X. Huang, R. Solasi, Y. Zou, M. Feshler, K. Reifsnider, D. Condit, S. Burlatsky and T. Madden, *Journal of Polymer Science Part B: Polymer Physics*, 2006, **44**, 2346-2357.

16. T. J. Peckham and S. Holdcroft, *Advanced Materials*, 2010, **22**, 4660-4660.

17. G. W.T., *Fuel Cell United States, Patent US 2913511*, 1959, **2**, 511.

18. D. A. Dixon, B. E. Smart, P. J. Krusic and N. Matsuzawa, *Journal of Fluorine Chemistry*, 1995, **72**, 209-214.

19. M. Eikerling and A. A. Kornyshev, *Journal of Electroanalytical Chemistry*, 2001, **502**, 1-14.

20. K. A. Mauritz and R. B. Moore, *Chemical Reviews*, 2004, **104**, 4535-4586.

21. H. Ward Andrew, C. Kendrick Thomas and C. Saam John, in *Copolymers, Polyblends, and Composites*, AMERICAN CHEMICAL SOCIETY, 1975, vol. 142, pp. 300-308.

22. J. Peron, A. Mani, X. Zhao, D. Edwards, M. Adachi, T. Soboleva, Z. Shi, Z. Xie, T. Navessin and S. Holdcroft, *Journal of Membrane Science*, 2010, **356**, 44-51.

23. A. Mani and S. Holdcroft, *Journal of Electroanalytical Chemistry*, 2011, **651**, 211-215.

24. K. D. Kreuer, *Journal of Membrane Science*, 2001, **185**, 29-39.

25. C. A. Edmondson, P. E. Stallworth, M. E. Chapman, J. J. Fontanella, M. C. Wintersgill, S. H. Chung and S. G. Greenbaum, *Solid State Ionics*, 2000, **135**, 419-423.

26. A. Ghielmi, P. Vaccarono, C. Troglia and V. Arcella, *Journal of Power Sources*, 2005, **145**, 108-115.

27. M. Gebert, A. Ghielmi, L. Merlo, M. Corasaniti and V. Arcella, *ECS Transactions*, 2010, **26**, 279-283.

28. L. Merlo, A. Ghielmi, L. Cirillo, M. Gebert and V. Arcella, *Separation Science and Technology*, 2007, **42**, 2891-2908.

29. A. S. Aricò, A. Di Blasi, G. Brunaccini, F. Sergi, G. Dispenza, L. Andaloro, M. Ferraro, V. Antonucci, P. Asher, S. Buche, D. Fongalland, G. A. Hards, J. D. B. Sharman, A. Bayer, G. Heinz, N. Zandonà, R. Zuber, M. Gebert, M. Corasaniti, A. Ghielmi and D. J. Jones, *Fuel Cells*, 2010, **10**, 1013-1023.

30. Y. Luan, H. Zhang, Y. Zhang, L. Li, H. Li and Y. Liu, *Journal of Membrane Science*, 2008, **319**, 91-101.

31. T. D. Gierke, G. E. Munn and F. C. Wilson, *J. Polym. Sci., Polym. Phys. Ed.*, 1981, **19**, 1687.

32. G. Gebel and J. Lambard, *Macromolecules*, 1997, **30**, 7914.

33. M.-H. Kim, C. J. Glinka, S. A. Grot and W. G. Grot, *Macromolecules*, 2006, **39**, 4775-4787.

34. K. Schmidt-Rohr and Q. Chen, *Nature Material*, 2008, **7**, 75-83.

35. S. J. Paddison, *Annual Review of Materials Research*, 2003, **33**, 289-319.

36. R. B. Moore and C. R. Martin, *Macromolecules*, 1989, **22**, 3594-3599.

37. K. D. Kreuer, M. Schuster, B. Obliers, O. Diat, U. Traub, A. Fuchs, U. Klock, S. J. Paddison and J. Maier, *Journal of Power Sources*, 2008, **178**, 499-509.

38. A. Siu, J. Schmeisser and S. Holdcroft, *The Journal of Physical Chemistry B*, 2006, **110**, 6072-6080.

39. M. G. Cupta, P. J. Joseph and P. A. Kohl, *Journal of Applied Polymer Science*, 2007, **105**, 2655-2662.

40. S. J. Paddison, R. Paul and T. A. Zawodzinski, *Journal of Chemical Physics*, 2001, **115**, 7753.

41. A. Roudgar, S. P. Narasimachary and M. Eikerling, *The Journal of Physical Chemistry B*, 2006, **110**, 20469-20477.

42. K.-D. Kreuer, *Chemistry of Materials*, 1996, **8**, 610-641.

43. K.-D. Kreuer, *Solid State Ionics*, 2000, **136-137**, 149-160.

44. P. Choi, N. H. Jalani, T. M. Thampan and R. Datta, *Journal of Polymer Science Part B: Polymer Physics*, 2006, **44**, 2183-2200.

45. K.-D. Kreuer, A. Rabenau and W. Weppner, *Angewandte Chemie International Edition in English*, 1982, **21**, 208-209.

46. P. H. Rieger, *Electrochemistry*, 1987, **Prentice-Hall: Englewood Cliffs, N.J.**

47. T. J. Peckham, J. Schmeisser, M. Rodgers and S. Holdcroft, *Journal of Materials Chemistry*, 2007, **17**, 3255-3268.

48. M. Eikerling, A. A. Kornyshev, A. M. Kuznetsov, J. Ulstrup and S. Walbran, *The Journal of Physical Chemistry B*, 2001, **105**, 3646-3662.

49. S. Paddison, in *Device and Materials Modeling in PEM Fuel Cells*, eds. S. Paddison and K. Promislow, Springer Berlin / Heidelberg, 2009, vol. 113, pp. 385-412.

50. J. Peron, D. Edwards, M. Haldane, X. Y. Luo, Y. M. Zhang, S. Holdcroft and Z. Q. Shi, *Journal of Power Sources*, 2011, **196**, 179-181.

51. G. A. Eisman, *Journal of Power Sources*, 1990, **29**, 389-398.

52. G. Gebel and R. B. Moore, *Macromolecules*, 2000, **33**, 4850-4855.

53. V. Arcella, C. Troglia and A. Ghielmi, *Industrial & Engineering Chemistry Research*, 2005, **44**, 7646-7651.

54. A. S. Arico, V. Baglio, A. Di Blasi, V. Antonucci, L. Cirillo, A. Ghielmi and V. Arcella, *Desalination*, 2006, **199**, 271-273.

55. L. Merlo, A. Ghielmi, L. Cirillo, M. Gebert and V. Arcella, *Separation Science and Technology*, 2007, **42**, 2891 - 2908.

56. J. Lin, Y. Liu and Q. M. Zhang, *Polymer*, 2011, **52**, 540-546.

57. D. Gorri, M. G. De Angelis, M. Giacinti Baschetti and G. C. Sarti, *Journal of Membrane Science*, 2008, **322**, 383-391.

58. M. G. De Angelis, S. Lodge, M. Giacinti Baschetti, G. C. Sarti, F. Doghieri, A. Sanguineti and P. Fossati, *Desalination*, 2006, **193**, 398-404.

59. S. J. Paddison and J. Elliott, *ECS Transactions*, 2006, **1**, 207-214.

60. S. J. Paddison and J. A. Elliott, *Physical Chemistry Chemical Physics*, 2006, **8**, 2193-2203.

61. J. Liu, N. Suraweera, D. J. Keffer, S. Cui and S. J. Paddison, *The Journal of Physical Chemistry C*, 2010, **114**, 11279-11292.

62. D. Wu, S. J. Paddison and J. A. Elliott, *Macromolecules*, 2009, **42**, 3358-3367.

63. S. Ahadian, H. Mizuseki and Y. Kawazoe, *Journal of Membrane Science*, 2011, **369**, 339-349.

64. D. Brandell, J. Karo, A. Liivat and J. Thomas, *Journal of Molecular Modeling*, 2007, **13**, 1039-1046.

65. I. H. Hristov, S. J. Paddison and R. Paul, *The Journal of Physical Chemistry B*, 2008, **112**, 2937-2949.

66. M. Adachi, T. Navessin, Z. Xie, B. Frisken and S. Holdcroft, *Journal of the Electrochemical Society*, 2009, **156**, B782-B790.

67. C. Chuy, V. I. Basura, E. Simon, S. Holdcroft, J. Horsfall and K. V. Lovell, *J Electrochem Soc*, 2000, **147**, 4453-4458.

68. V. Arcella, A. Ghielmi and G. Tommasi, *Annals of the New York Academy of Sciences*, 2003, **984**, 226-244.

69. T. Astill, Z. Xie, Z. Q. Shi, T. Navessin and S. Holdcroft, *Journal of the Electrochemical Society*, 2009, **156**, B499-B508.

70. V. I. Basura, P. D. Beattie and S. Holdcroft, *J Electroanal. Chem.*, 1998, **458**, 1-5.

71. P. D. Beattie, V. I. Basura and S. Holdcroft, *J Electroanal. Chem.*, 1999, **468**, 180-192.

72. Z. Xie and S. Holdcroft, *Journal of the Electroanalytical Chemistry*, 2004, **568**, 247–260.

73. T. Biegler, D. A. J. Rand and R. Woods, *J Electroanal. Chem.*, 1971, **29**, 269-277.

74. S. J. Paddison and J. A. Elliott, *The Journal of Physical Chemistry A*, 2005, **109**, 7583-7593.

75. P. D. Beattie, V. I. Basura and S. Holdcroft, *Journal of Electroanalytical Chemistry*, 1999, **468**, 180-192.

76. V. I. Basura, C. Chuy, P. D. Beattie and S. Holdcroft, *Journal of Electroanalytical Chemistry*, 2001, **501**, 77-88.

77. A. S. Aricò, A. Stassi, E. Modica, R. Ornelas, I. Gatto, E. Passalacqua and V. Antonucci, *Journal of Power Sources*, 2008, 178, 525-536.

Appendix: Sample Data

The following is sample data for the calculations that were performed in chapter 2

Table A-1 Data summary for short side chain (SSC) membranes and long side chain (LSC) membranes under fully hydrated condition at room temperature

Membrane	X_v (%)	λ (mol H_2O/ mol-SO_3H)	[-SO_3H] (M)	σ_{H+} (mS/cm)	$\mu'_{H+} \times 10^3$ ($cm^2\ s^{-1}\ V^{-1}$)
SSC-1.3	56±7	15.18±0.97	2.04±0.14	115±2.83	0.58±0.02
SSC-1.4	62±3	16.65±0.16	2.80±0.14	87.7±2.05	0.50±0.02
SSC-1.5	75±9	17.68±0.26	2.36±0.23	91.9±1.27	0.40±0.03
LSC-0.94	28±2	10.6±0.49	1.50±0.03	81.9±0.42	0.43±0.004
LSC-1.05	28±1	15.35±0.50	1.23±0.33	93.8±2.05	0.55±0.02
LSC-1.06	28.8±3	13.85±0.57	1.15±0.08	95.3±0.71	0.57±0.05
LSC-1.09	29.2±2	13.80±0.21	1.23±0.18	91.7±1.91	0.68±0.03
LSC-1.13	29.5±2	16.25±0.86	1.02±0.09	107±2.47	0.73±0.003
Nafion®211	26±4	12.69±0.27	1.26±0.03	78.8±0.1	0.43±0.009